The Genus One Helicoid and the Minimal Surfaces that led to its discovery

David Hoffman Hermann Karcher Fusheng Wei

Introduction

Around 1780, soon after Lagrange derived the minimal surface equation, Meusnier found the first nonplanar solutions: Euler's catenoid and the helicoid. More than 200 years later, in 1980, the catenoid was still the only known finite total curvature embedded minimal surface and the helicoid was the only known *infinite* total curvature embedded minimal surface of *finite* topology. First, the finite total curvature situation changed. Chen-Gackstatter [CG] found an immersed torus with one end and - soon after that - Costa [C] found an embedded torus with three ends. We now know that for every genus ≥ 1, there exists a one-parameter family of embedded finite total curvature minimal surfaces with three ends ([HM]), and we have some more examples - less well understood - with four and five ends. ([CHM,BW,W1,W2,HK]).
In this paper we describe the construction of a minimally embedded torus with *one* end and *infinite* total curvature ([HKW]). The (elliptic) Gauss map of this surface has an essential singularity at the puncture and this makes the surface fundamentally different from all previous embedded examples. The other infinite total curvature and finite topology embedded minimal surface, the helicoid, can be described with the exponential map as Gauss map, i.e. with an essential singularity. The new surface is substantially more complicated than the helicoid because it does *not* cover a *finite* total curvature surface in a flat spaceform (namely in $\mathbb{R}^2 \times \mathbb{S}^1$ in the case of the helicoid). Therefore it cannot be described on a quotient surface in terms of a *meromorphic* Gauss map. (In the case of the helicoid, $g(z) = z$ on $\mathbb{C} - \{0\}$.)

It is a pleasure to contribute this paper to a volume dedicated to Dick Palais. For one of us he is the only non-specialist who was seriously interested in our work and was willing to spend many hours discussing it. To another he has been a long-term source of good advice, both mathematical and computational. The topic is also appropriate for another reason. Dick has worked hard to help make computers more easily usuable by mathematicians, and the intuition to achieve the results we describe was significantly influenced by computer output. As friends we congratulate Dick and hope he enjoys this volume.

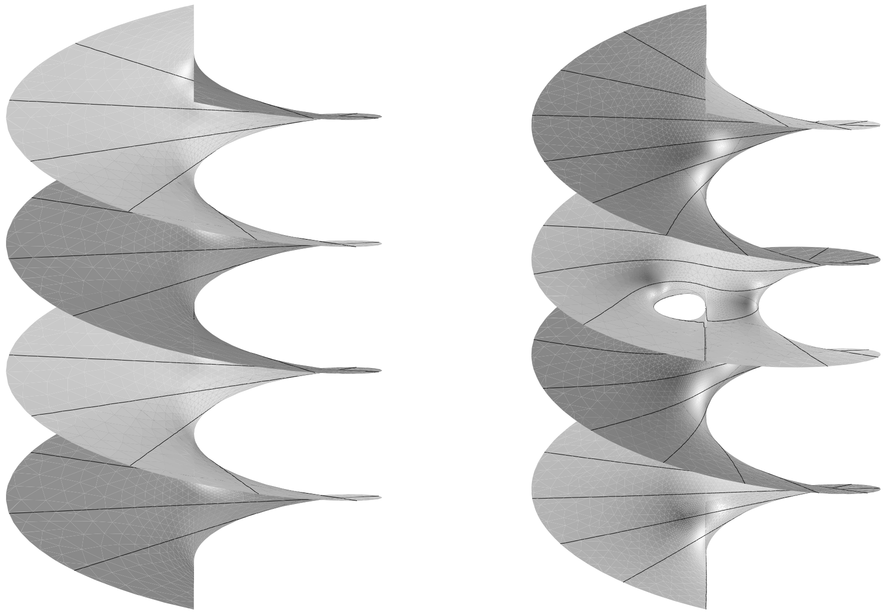

Figure 1
Helicoid (left), Helicoid with handle (right)

1. Overview

1.1 How does one find such a new surface?

Over the past five years, we were led through the study of more and more complicated examples to the discovery of the genus one helicoid. We want to explain this story in steps of increasing detail. The surfaces we will discuss are constructed via their Weierstrass representations in roughly the following way: *Assume* first that one has a "qualitatively correct" picture of the expected minimal surface. It is possible to deduce, perhaps up to several parameters, the underlying Riemann surface structure, compatible with the qualitative picture. Then we interpret the minimal surface as an excellent visualization of its Gauss map from the Riemann surface to the Riemann sphere. As long as we are dealing with *meromorphic* Gauss maps, a qualitatively correct visualization is precise enough to determine the Gauss map (again, possibly, up to a few parameters). With the help of the ends and the vertical points of the Gauss map, we then can determine a family of Weierstrass data that *defines* the coordinate differentials of candidates for the expected minimal surface. Finally, the undetermined parameters have to be adjusted so that the integrals of these coordinate differentials along closed paths on the Riemann surface give closed curves in $\mathbb{R}^3$. (This is the so-called period problem.)
The reader will not be surprised to learn that there are some problems with this "method". First of all, the initial picture has to be "qualitatively correct,"

otherwise one will deduce Weierstrass data that do not give the surface. Several things can go wrong and, in the end, the period problem may not have a solution. There are at present only two theorems that prevent doomed attempts by giving a priori impossible properties: A theorem of Lopez-Ros [LR] says that the only nonplanar, finite total curvature, embedded, finitely punctured *sphere* is the catenoid - more punctures are impossible; and a theorem of R. Schoen [SC] says that the only embedded, finite total curvature minimal surface with *two* ends is the catenoid - *higher genus* is impossible.
When a Gauss map has an essential singularity, there is another serious problem: we don't know how to recognize a function with an essential singularity from a "qualitatively correct" picture. In fact, we do not even know how to do this from a perfect picture. The Weierstrass representation has to be generalized to handle this difficulty.

1.2 Which surfaces contributed to our discovery?

In the first few steps we go from surfaces of Scherk (1835) to a singly-periodic surface of Hoffman and Wei, which looks like a helicoid with an additional handle in each fundamental piece of the translational symmetry group. All the surfaces we will describe have *meromorphic* Gauss maps. For the last step, we need a generalization of the Weierstrass representation. The first examples that illustrated the usefulness of such a generalization were twisted deformations of Scherk's saddle-tower surface. For these surfaces, the Gauss map is multivalued on the parametrizing Riemann surface because of screw-motion symmetries of the minimal surface. However, the logarithmic differential dg/g is well-defined and the multivalued Gauss map is obtained as $\exp(\int dg/g)$ (the integration taking place on a simply-connected fundamental piece) [K1].
We will explain how we were led to assume that such "generalized" Weierstrass data for the genus one helicoid were *meromorphic* differential forms, and therefore that they could be deduced. This data gave us the desired minimal surface; its Gauss map has one zero, one simple pole and one essential singularity on a specific rhombic torus. We had not met such a function before, but we have since learned that it is a specific Baker-Akhiezer function. For the Weierstrass representations of those surfaces that we wish to explain in detail we need some specific information about elliptic functions, especially on rhombic tori. This is found in Section 3, which may be read independently from the rest of the paper.

2. Surfaces that are (in retrospect) related to the genus one helicoid.

We discuss first the surfaces that educated our intuition.

2.1 Scherk's surfaces.

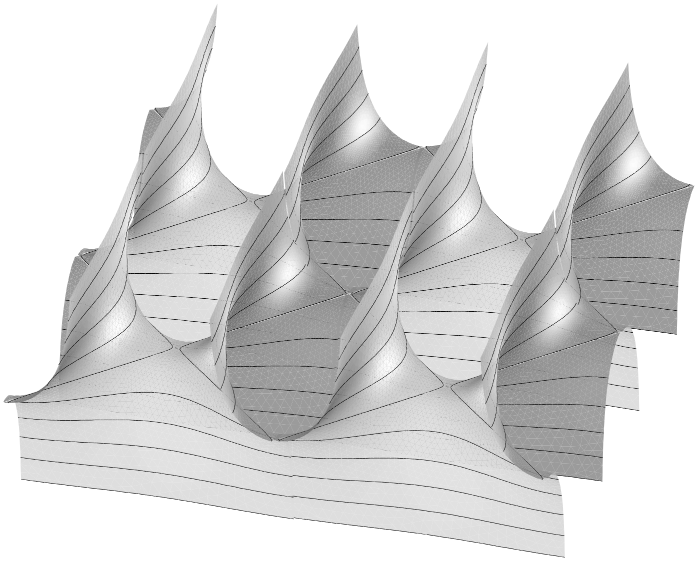

Figure 2
Scherk's doubly-periodic surface

If one divides Scherk's doubly-periodic minimal surface [S] (or its conjugate, the singly-periodic Scherk saddle tower) by its translational symmetries, then one obtains a sphere, punctured in four points, on which the Gauss map is of degree one. After a Möbius-reparametrization, we can assume $g(z) = z$. After a rotation in $\mathbb{R}^3$, the values of g at the four punctures are $g = \pm e^{\pm i\pi/4}$. We call the vertical height function x_3 and denote its complex differential by $dh := dx_3 - i dx_3 \circ R_{\pi/2}$. (Here, $R_{\pi/2}$ is the 90^0 rotation that gives the complex structure in each tangent plane.) From the Weierstrass data g, dh, the minimal surface is obtained via

2.1.1. The "Weierstrass-integral":

$$Re \int \left(\frac{1}{2}\left(\frac{1}{g} - g\right), \frac{i}{2}\left(\frac{1}{g} + g\right), 1 \right) dh.$$

2.1.2. Riemannian metric:

$$ds = \left(|g| + \frac{1}{|g|} \right) |dh|.$$

Using the metric we can now determine dh: This differential form has to have simple zeros at the zero and the pole of g and therefore four, necessarily simple, poles, necessarily at the punctures. That is,

$$dh = re^{i\varphi}\frac{1}{z^2+z^{-2}}\cdot\frac{dz}{z}.$$

The scaling parameter r controls only the size of the minimal surface; we ignore it. It remains to verify that, for $\varphi = 0$, we get Scherk's saddle tower and, for $\varphi = \pi/2$, his doubly-periodic surface; we omit this (since we want to concentrate on the determination of Weierstrass data from qualitatively correct pictures. See [K1,K2,HW] for further details.). Scherk's surfaces can be deformed by moving the punctures to $\pm e^{\pm i\alpha}, 0 < \alpha \leq \pi/4$. Apart from these related surfaces, his doubly-periodic one remained the only such example for 150 years.

2.2 Doubly-periodic punctured tori.

The next examples were found using the following qualitatively correct picture: Karcher [K1] assumed that one could have minimal surfaces which look like a fence of Scherk saddle towers "glued together", either along vertical straight lines or along vertical planar symmetry curves. Division by the translational symmetries of such a surface gives a torus with four punctures. The orientation-reversing symmetry from the rotation around a vertical line (resp. reflection in a vertical planar symmetry curve) descends to the torus and has a fixed point set with two components (from a pair of neighbouring symmetry lines; note also that their symmetries compose to give a period translation). The torus is therefore a rectangular torus. On it, the Gauss map is of degree-two. At the points where a straight line meets a planar symmetry curve the Gauss curvature is zero; i.e. we have a branch point of the Gauss map. The four branch points of a degree two elliptic function form a half-period lattice, and two such functions with the same branch points differ by a Möbius transformation. This Möbius transformation determines where on the torus the zeros and poles of the function are located. It is convenient to rotate the surface in $\mathbb{R}^3$ so that the Gauss map is vertical at the four punctures. The Riemannian metric (2.1.2) shows that dh can have neither poles nor zeros outside the punctures and no zeros at the punctures; it therefore is proportional to the standard holomorphic form on the torus: $dh = re^{i\varphi}dz,\ z \in \mathbb{C}/\Gamma$, Γ a lattice.
It remains to determine the Möbius transformation and to consider the period problem. For the Möbius transformation one has many choices, since the surfaces turn out to be quite deformable: one does not need to take Scherk's orthogonal saddle tower in our initial qualitatively correct picture, but any of the deformed saddle towers (with non-orthogonal ends) will do. Also, the relative height between the first and the second tower is a free parameter. Since we also can recognize symmetries of the minimal surface from its Weierstrass data, we can see that the period problem is solved automatically for the most symmetric choices of the Möbius transformation (e.g. $g = (\wp_g - i)/(\wp_g + i)$ on any rectangular torus, where $\wp_g$ is the geometrically normalized Weierstrass $\wp$-function. See Section 3). We will be more detailed later, but since these initial examples are published [K1] we wish to emphasize only the noncomputational parts of the arguments.

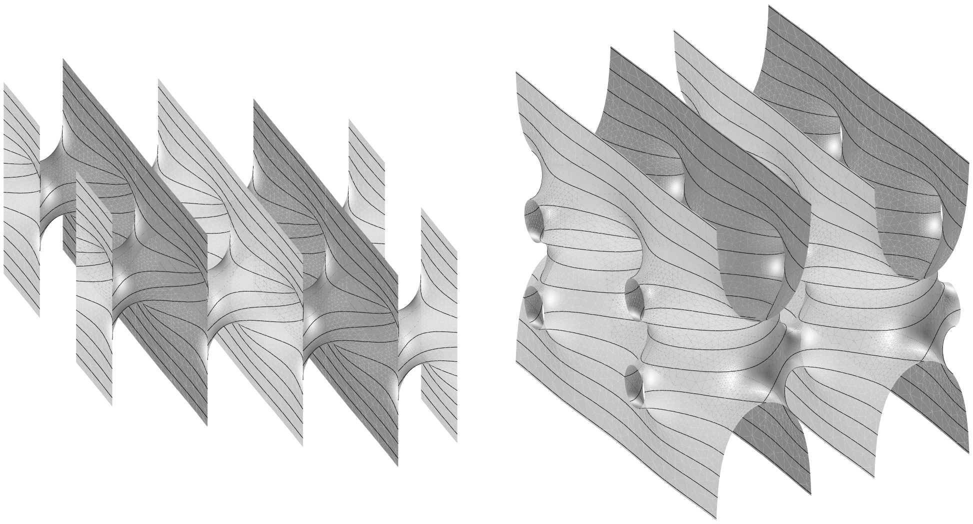

Figure 3

Karcher's genus one doubly-periodic surface (left), and Wei's genus two doubly-periodic surface (right)

2.3 Doubly-periodic examples of genus two.

The next experience was gained from triply-periodic minimal surfaces. They could be modified rather easily into more complicated ones by adding handles, as if "minimal surface surgery" were possible. With more effort, these ideas could be used to modify singly-periodic and finite total curvature minimal surfaces. However, the doubly-periodic ones resisted modification. In restrospect, the reason for this is simple to see; the period problem had always become simpler if one assumed the expected minimal surface to be as symmetric as possible, while remaining compatible with a qualitative picture. It was Wei [WE] who found that the modifications did succeed on the known doubly-periodic minimal tori if one added only half as many handles as the most symmetric treatment would require. He obtained embedded, doubly-periodic minimal surfaces, parametrized by genus two Riemann surfaces. The moduli space of genus two surfaces has three complex dimensions, and of course its elements are not as well-known by individual names (e.g. square, rhombic, hexagonal) as the tori are. From a qualitatively correct picture of a desired surface, including knowledge of its symmetries, one has to determine the compatible Riemann surface structure(s), which in turn must support meromorphic functions that are suitable candidates for the Gauss map. When the genus is greater than one, this is a much more serious part of the problem.

In the present cases (and in many others), we have two natural meromorphic functions without common branch points on the Riemann surface. Together they supply an atlas of holomorphic coordinates. The coordinate changes are given by an algebraic relation between these functions, and this relation, in turn, defines the Riemann surface in the best known, the "classical", way. One of these natural functions is the Gauss map, of degree 3. To see the other one, observe that the planar symmetry lines cut (a qualitatively correct picture of) the surface into simply-connected right angle pentagons. The 180^0 rotations around the normals at the vertices are orientation-preserving isometries of the minimal surface. If we divide by the group generated by the vertical rotation and then by the translations, we get the sphere as quotient Riemann surface. The quotient map of degree two sends each of the above pentagons to a quarter-sphere. The Gauss map is vertical on three of the vertices and has values in the set $\{\pm 1, \pm i\}$ at the other two. We Möbius-normalize the quarter-sphere to be the first quadrant; specifically, we send the two vertices with horizontal normal to $0, \infty$ and we send the other three to $\lambda < 1 < \lambda_1$ on $\mathbb{R}^+$, where λ, λ_1 are two conformal parameters. In this normalized form, we call the projection map Z. The functions

$$g^2 \quad \text{and} \quad (Z-\lambda)(Z-\lambda_1)(Z+1)/(Z+\lambda)(Z+\lambda_1)(Z-1)$$

have the same zeros and poles; i.e. they are proportional, and they agree at the other vertices where g^2 is ± 1. Therefore, the equation

$$g^2 = \frac{(Z-\lambda)(Z-\lambda_1)(Z+1)}{(Z+\lambda)(Z+\lambda_1)(Z-1)}$$

describes our Riemann surfaces as hyperelliptic curves, *with one of the defining functions the candidate for the Gauss map!* Finally, the qualitatively correct picture shows that the Gauss map is ± 1 at the puncture; i.e. the puncture has to be at $Z = \pm a$, where $(a+\lambda)(a+\lambda_1)(a-1) = (a-\lambda)(a-\lambda_1)(a+1)$ or

$$a^2 \cdot (\lambda + \lambda_1 - 1) = \lambda \cdot \lambda_1.$$

Now one sees immediately from the Riemannian metric (2.1.2), that dh needs simple zeros at the vertical points of g and simple poles where $Z = \pm a$. This determines

$$dh = re^{i\varphi} \cdot \frac{dZ}{Z^2 - a^2}.$$

Again r is the irrelevant scaling factor and $\varphi = 0$ picks the desired surface in the associate family, since dh has to be real on the tangent vectors of the vertical symmetry lines.

At this point we have derived a 2-parameter (λ, λ_1)-family of Weierstrass data and have to turn to the period problem. There are not enough symmetries to solve it automatically, but Wei [WE] shows that $\lambda_1(\lambda)$ can be chosen so that for each $\lambda \in (0, 1)$ the period problem is solved. We do not go into further details here because the main lesson of this example - less symmetry is sometimes better than more - can be understood without the details. We gave the noncomputational part of the derivation to illustrate - as in all other cases - what we mean by the dictum: "Deduce a candidate for the Weierstrass representation from a qualitatively correct picture."

3. A supply of basic elliptic functions

At this point the narration should continue with a discussion of Karcher's modification of Scherk's doubly-periodic surface of genus 1, which was suggested by the "less than maximal symmetry" approach in the previous example of Wei. However, with this next example, we come close enough to our final surface so that we also want to explain how the period problem is solved. Since all the remaining surfaces will be parametrized by punctured tori we have to deal more explicitly with elliptic functions. We give a self-contained introduction that is tailored to our needs. In particular:

(i) The symmetries (or functional equations) of degree two elliptic functions are usually expressed in terms of Möbius transformations of the Riemann sphere. We want these Möbius transformations to be *isometric* rotations; we will in fact realize them as rotations about the coordinate axes of the sphere in $\mathbb{R}^3$, given in $\mathbb{C}$ as $z \to \pm z^{\pm 1}$. In the special case of rectangular or rhombic tori— the ones with "complex conjugation"— we realize the corresponding Möbius reflections as *isometric* reflections in coordinate planes (i.e. $z \to \pm \bar{z}$, $z \to 1/\bar{z}$);

(ii) We want to build more complicated functions by multiplying simple ones with known zeros and poles (as we do with rational functions). The classical approach treats only two functions in a distinguished way, namely the ones that go into the equation of the surface. We need a larger collection of distinguished functions together with their mutual relations.

3.1 Construction of degree-two elliptic functions.

3.1.1. Quotient functions. The typical degree two elliptic function can be constructed as follows. View the torus T as $\mathbb{C}/\Gamma$. Any 180^0 rotation r of $\mathbb{C}$ around a point c_0 induces an orientation-preserving involution of T with four fixed points (which are given in $\mathbb{C}$ as $c_0 + \frac{1}{2} \cdot \Gamma$, a "half-period lattice"). The quotient surface is the Riemann sphere since $\chi(T/r) = 2$. This follows either from $0 = \chi(T) = 2 \cdot \chi(T/r) - 4$ or by applying Euler's $\chi = V - E + F$ to the tessalation of T by the four parallelograms whose vertices are the fixed points of r and to the quotient tessalation, which has $F = 2$ quadrilaterals, $E = 4$ edges and $V = 4$, the fixed points. At this point the quotient sphere is only a conformal sphere, not yet the standard sphere in $\mathbb{R}^3$ which is identified with $\mathbb{C} \cup \{\infty\}$ via stereographic projection. But after we call three arbitrary points of the quotient sphere $0, 1, \infty$ we have a unique identification with the standard sphere. We then call the quotient map a function. Any two such choices of $0, 1, \infty$ give two functions that differ by a Möbius transformation. Moreover, if two degree two elliptic functions f_1, f_2 on T have one branch point $c_0 \in T$ in common then, all their branch points agree. Here is a proof. We may assume $f_1(c_0) = 0$, $f_2(c_0) = 0$, and also that f_1 has been constructed as above with a double pole at one of its other three branch points, say c_1. If necessary, replace f_2 by $f_2/(f_2 - f_2(c_1))$ so that $f_2(c_1) = \infty$. Then f_1/f_2 has at most one pole (at c_1) and one zero, hence it is constant, q.e.d..

We may summarize this as follows: Any two degree two elliptic functions on the same torus differ by a translation of the torus—which positions their branch points— and by a Möbius transformation of the sphere—which positions $0,\ 1,\ \infty$.

3.1.2. Remark. This approach shows that the cross-ratio of the four branch values (in suitable order) depends only on the torus; it is called the *modular invariant* of the torus and it is usually computed from the finite branch values of the Weierstrass $\wp$-function as $(e_1 - e_3)/(e_2 - e_3)$. The differential equations below for our elliptic functions will depend only on this modular invariant.

3.1.3. Symmetries. The following simple observation is responsible for the symmetries of the degree two elliptic functions: Given one 180^0 rotation r of the torus T , there are three other 180^0 rotations of T which *permute the fixed points* of r . This means for the quotient map $f : T \to T/r$:

$$f \circ \text{ Torus-rotation}_k = \text{ Möbius-involution}_k \circ f, \qquad k = 1, 2, 3,$$

since on the left side we have degree two maps $T^2 \to S^2$ with the same branch points as f. One of our aims is to have these Möbius involutions as simple as possible; we will achieve them as $z \to \pm z^{\pm 1}$.

3.1.4. Special choices. We now use the observations above to construct three functions that have the same distribution of simple zeros and poles as Jacobi's degree two elliptic functions. A fourth function will be constructed with a double zero and a double pole. On the square torus it is, up to scaling, the Weierstrass $\wp$-function. On other tori it is somewhat different and the values are changed: $a \cdot \wp + b$. We facilitate our description by choosing a fundamental parallelogram for the torus, which has its midpoint at $0 \in \mathbb{C}$. (We will also refer to this point as a point $0 \in T = \mathbb{C}/\Gamma$.) The rotational position and the scaling will be specified later. The half-period lattice $0 + \frac{1}{2} \cdot \Gamma$ determines the vertices and the midpoints of the edges of the chosen fundamental parallelogram. To specify a function of degree two we have to give its branch points in the fundamental parallelogram (a half-period set marked by a $\bullet$ in the figure) and we have to specify three points that are to go to $0, \infty$ and either 1 or i. It is convenient to write these *values* in the *domain* parallelogram; the choice of their position, of course, determines the functional relations. To simplify building more functions by multiplication, we will always choose the zeros and poles at the half-period points. By the definition of a quotient map we do not change the values of the (quotient) function if we rotate the torus around the chosen branch points. This means that, for the Jacobi-type functions, the branch points have to be chosen as midpoints between the zeros (and hence also as midpoints between the poles). The finite value 1 (resp. i) is placed at a midpoint between a zero and a pole because 180^0 rotation of the Riemann sphere around 1 interchanges $0, \infty$. This choice is responsible for the simplicity of the Möbius transformation in the functional relations. In the case of the Jacobi-type functions and for the geometrically normalized Weierstrass $\wp$-function we denote the 180^0 rotations of the torus and their quotient functions as follows.

$$\text{rotations: } r_{D}, r_{E}, r_{F}, r_{P}; \qquad \text{functions: } \mathfrak{J}_{D}, \mathfrak{J}_{E}, \mathfrak{J}_{F}, \wp_g .$$

The following diagrams *define our four functions*, which, of course, must satisfy $f \circ r = f$.

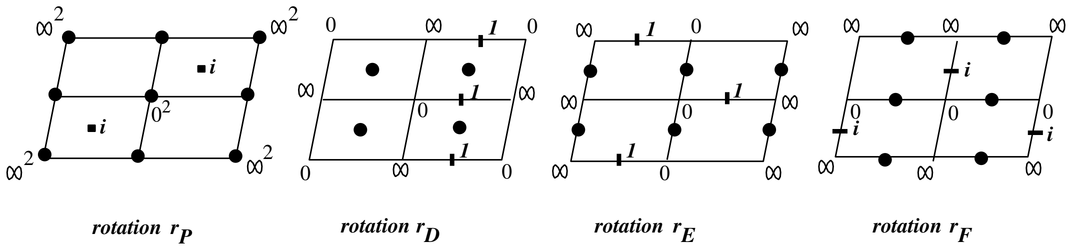

$\wp_g$ $\qquad\qquad$ $\mathfrak{J}_D$ $\qquad\qquad$ $\mathfrak{J}_E$ $\qquad\qquad$ $\mathfrak{J}_F$

3.1.5. Functional equations. Recall that each of the four rotations permutes the fixed points of the other rotations and that this is the source of the functional equations. In each case we get the first relation from the rotation around the point where the finite value 1 (resp. i)) was chosen:

$$\mathfrak{J}_D \circ r_F = \frac{1}{\mathfrak{J}_D}, \quad \text{values } \pm 1 \text{ at fixed points of } r_F;$$
$$\mathfrak{J}_E \circ r_F = \frac{1}{\mathfrak{J}_E}, \quad \text{values } \pm 1 \text{ at fixed points of } r_F;$$
$$\mathfrak{J}_F \circ r_E = \frac{-1}{\mathfrak{J}_F}, \quad \text{values } \pm i \text{ at fixed points of } r_E;$$
$$\wp_g \circ r_D = \frac{-1}{\wp_g}, \quad \text{values } \pm i \text{ at fixed points of } r_D.$$

This says that the Jacobi-type functions are odd, and that $\wp_g$ is even:

$$\mathfrak{J}_D \circ r_P = -\,\mathfrak{J}_D, \quad \wp_g \circ r_P = \wp_g\,.$$

The diagrams, completed with these first special values, look like this:

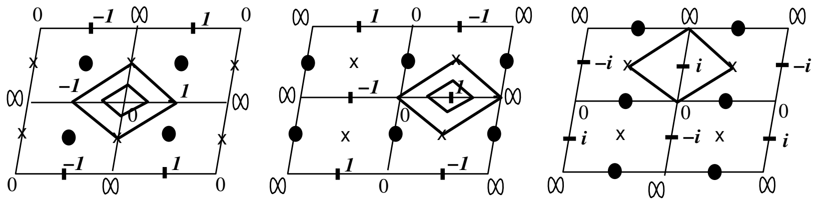

$\mathfrak{J}_D$ $\qquad\qquad$ $\mathfrak{J}_E$ $\qquad\qquad$ $\mathfrak{J}_F$

We read off the relations that (3.1.3) promised:

$$\mathfrak{J}_D \circ r_E = \frac{-1}{\mathfrak{J}_D}; \quad \mathfrak{J}_E \circ r_D = \frac{-1}{\mathfrak{J}_E}; \quad \mathfrak{J}_F \circ r_D = \frac{+1}{\mathfrak{J}_F}.$$

In the diagram, we have marked by $\times$ the fixed points of the relevant rotations. At these fixed points ($\times$) the functions have *values* which are fixed under the corresponding Möbius-involution $\mathfrak{J}_D \to \pm 1/\,\mathfrak{J}_D$, namely ± 1, resp. $\pm i$. The distribution of the $\pm$signs is a matter of orientation. For example in the case of $\mathfrak{J}_D$, the parallelogram disk around $0 \in T$ that is indicated in the figure is mapped by $\mathfrak{J}_D$ biholomorphically to a disk around $0 \in \mathbb{C}$ that has $1,\ i,\ -1,\ -i$ on its boundary in the positive order. Therefore we have these values in the same order around $0 \in T$. The same argument applies to $\mathfrak{J}_E,\ \mathfrak{J}_F$.

3.1.6. Branch values. So far we have not seen anything that is specific to the torus under consideration. We have already mentioned that the cross-ratio of the branch values is the modular invariant which distinguishes the tori. So, in each of the three Jacobi-type functions, $\mathfrak{J}_D, \mathfrak{J}_E, \mathfrak{J}_F$, we first give one branch value a name: D, E, F, respectively. Then since all the functional equations (3.1.3) were shown to use the Möbius involutions $z \to \pm z^{\pm 1}$ we find the other branch values as $\pm(D, E, F)^{\pm 1}$. We summarize by giving the fundamental parallelograms with all the special values. The subparallelogram with the first named branch point in its right upper corner is shaded. Rotation around a zero or pole sends a branch value B to $-B$; rotation around points with value ± 1 sends B to $1/B$; and rotation around $\pm i$ sends B to $-1/B$.

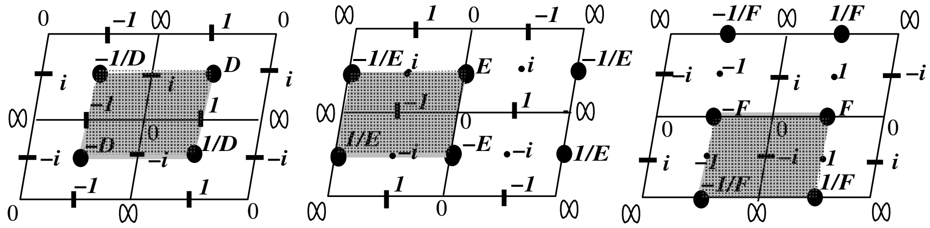

$\mathfrak{J}_D$ $\qquad$ $\mathfrak{J}_E$ $\qquad$ $\mathfrak{J}_F$

3.1.7. Relations modulo translations. To emphasize the close relation between these functions we also give the Möbius transformations that transform these functions, modulo torus translations, into one another. We choose the translations that map one of the shaded subparallelograms to another one. The translated functions have the same branch points and are therefore Möbius-related:

$$\mathfrak{J}_E \circ \text{translation}_1 = \frac{\mathfrak{J}_D - 1}{\mathfrak{J}_D + 1}, \quad \mathfrak{J}_F \circ \text{translation}_2 = i \cdot \frac{\mathfrak{J}_D - i}{\mathfrak{J}_D + i},$$
$$\mathfrak{J}_F \circ \text{translation}_3 = -\frac{\mathfrak{J}_E - i}{\mathfrak{J}_E + i}.$$

In particular, this shows the relation of the branch values:

$$E = \frac{D-1}{D+1}, \quad F = i \cdot \frac{D-i}{D+i}, \quad F = -\frac{E-i}{E+i}.$$

Finally we observe that $\wp_g$ and $\mathfrak{J}_E \cdot \mathfrak{J}_F$ have the same zeros and poles and agree where $\wp_g = i$. This gives the geometrically normalized Weierstrass $\wp$-function. Its Möbius relation with $\mathfrak{J}_D$ and its diagram of special values are as follows:

$$\wp_g \circ \text{translation}_4 = \text{Möbius}_4(\mathfrak{J}_D) := -i \cdot \frac{\mathfrak{J}_D + D}{\mathfrak{J}_D - D}, \quad \wp_g = \mathfrak{J}_E \cdot \mathfrak{J}_F$$

with one finite branch value $P = \text{Möbius}_4(1/D) = i(D^2+1)/(D^2-1)$.

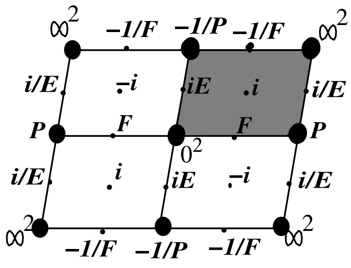

$$\wp_g = \mathfrak{J}_E \cdot \mathfrak{J}_F$$

3.1.8. Remark. We compute for later use the cross-ratio of the branch values:

$$1 + 4(D^2 + D^{-2} - 2)^{-1} = (E^2 + E^{-2} + 2)/4 = -4(F^2 + F^{-2} - 2)^{-1} = -P^2$$

and recall once more that it is the classical modular invariant of the torus.

3.2 Functional relations between the four functions.

3.2.1. Biquadratic Relations. The most common description of a Riemann surface is in terms of an algebraic relation between two functions (usually called z, w) on the Riemann surface. One may interpret the functions as (local) coordinates — away from their branch points of course—and the algebraic relation is a description of the change of coordinates. We can take any pair of our degree two elliptic functions and find a biquadratic relation between them. The following list of relations is immediately verified since both sides have the same zeros and the same poles and agree at another point (a branch point of the function involved on the left).

$$\begin{aligned}
\mathfrak{J}_D - \frac{1}{\mathfrak{J}_D} &= \frac{D-1/D}{2i}(\mathfrak{J}_E - \frac{1}{\mathfrak{J}_E}) = \frac{2i}{E-1/E}(\mathfrak{J}_E - \frac{1}{\mathfrak{J}_E}) \\
\mathfrak{J}_D + \frac{1}{\mathfrak{J}_D} &= \frac{D+1/D}{2}(\mathfrak{J}_F + \frac{1}{\mathfrak{J}_F}) = \frac{2}{F+1/F}(\mathfrak{J}_F + \frac{1}{\mathfrak{J}_F}) \\
\mathfrak{J}_E + \frac{1}{\mathfrak{J}_E} &= \frac{2}{F-1/F}(\mathfrak{J}_F - \frac{1}{\mathfrak{J}_F}) = \frac{E+1/E}{2i}(\mathfrak{J}_F - \frac{1}{\mathfrak{J}_F}) \\
\frac{D^2}{{\mathfrak{J}_D}^2} &= \frac{\wp_g - 1/\wp_g - P + 1/P}{2i - P + 1/P} = D^2 \cdot \frac{\wp_g - 1/\wp_g - P + 1/P}{F - 1/F - P + 1/P}
\end{aligned}$$

As an example, let the branch value D be given and rename $w = \mathfrak{J}_D, z = \mathfrak{J}_E$. The first equation then looks more familiar

$$(w - \frac{1}{w})/(D - \frac{1}{D}) = (z - \frac{1}{z})/(2i),$$

but we cannot immediately recover all our information about $\mathfrak{J}_D, \mathfrak{J}_E$ from this equation, and, of course, there are no relations with other functions.

3.2.2. Logarithmic derivatives. Another common choice of a pair of functions to describe a torus is to take a degree two elliptic function together with its logarithmic derivative. In the following list of relations the functions on both sides have the same zeros and poles; moreover, the first term of their Laurent expansion at $0 \in \mathbb{C}$ is the same — hence they agree. First we express the logarithmic derivative of the Jacobi type functions in terms of other functions; then we differentiate $\wp_g = \mathfrak{J}_E \cdot \mathfrak{J}_F$; we also note that $\wp_g + 1/\wp_g$ is a derivative; finally we give the differential equations:

$$
\begin{aligned}
\frac{\mathfrak{J}_F{}'}{\mathfrak{J}_F} &= \mathfrak{J}_D{}'(0) \cdot (\frac{1}{\mathfrak{J}_D} - \mathfrak{J}_D) = \mathfrak{J}_D{}'(0) \frac{-2i}{1/E - E} \cdot (\frac{1}{\mathfrak{J}_E} - \mathfrak{J}_E) \\
\frac{\mathfrak{J}_E{}'}{\mathfrak{J}_E} &= \mathfrak{J}_D{}'(0) \cdot (\frac{1}{\mathfrak{J}_D} + \mathfrak{J}_D) = \mathfrak{J}_D{}'(0) \frac{2}{1/F + F} \cdot (\frac{1}{\mathfrak{J}_F} + \mathfrak{J}_F) \\
\frac{\mathfrak{J}_D{}'}{\mathfrak{J}_D} &= \mathfrak{J}_E{}'(0) \cdot (\frac{1}{\mathfrak{J}_E} + \mathfrak{J}_E) = \mathfrak{J}_F{}'(0) \cdot (\frac{1}{\mathfrak{J}_F} - \mathfrak{J}_F) \\
\frac{\wp_g{}'}{\wp_g} &= \frac{\mathfrak{J}_E{}'}{\mathfrak{J}_E} + \frac{\mathfrak{J}_F{}'}{\mathfrak{J}_F} = \mathfrak{J}_D{}'(0) \cdot \frac{2}{\mathfrak{J}_D} \\
\left(\frac{1}{\mathfrak{J}_D}\right)' &= -\frac{\mathfrak{J}_D{}'}{\mathfrak{J}_D{}^2} = -\frac{\wp_g{}''(0)}{2\,\mathfrak{J}_D{}'(0)} \cdot (\wp_g + \frac{1}{\wp_g})
\end{aligned}
$$

3.2.3. Differential equations. The three Jacobi type functions have the same differential equation in terms of one of their branch values B. (Recall that $B^2 + B^{-2}$ can be expressed by the modular invariant.)

$$
\begin{aligned}
\left(\frac{\mathfrak{J}'}{\mathfrak{J}}\right)^2 &= \mathfrak{J}'(0)^2 \cdot (\mathfrak{J}^2 + \mathfrak{J}^{-2} - B^2 - B^{-2}) \\
\left(\frac{\wp_g{}'}{\wp_g}\right)^2 &= -2\,\wp_g{}''(0) \cdot (\wp_g - \frac{1}{\wp_g} - P + \frac{1}{P})
\end{aligned}
$$

We repeat that these relations hold because both sides have the same zeros and the same poles, and their Laurent expansions at $0 \in \mathbb{C}$ agree. Note that at this point the derivatives at $0 \in \mathbb{C}$ in the above relations are not yet determined, because we have not fixed the scaling size and the rotational position of the fundamental parallelogram in $\mathbb{C}$. If we fix this derivative at 0 in *one* of the differential equations, then the size and rotational position of the fundamental domain and also the derivative at 0 of each of the other functions are chosen. Their relation is obtained by comparing Laurent expansions at $0 \in \mathbb{C}$ in the biquadratic equations in (3.2.1):

$$
\begin{aligned}
\mathfrak{J}_E{}'(0) &= \frac{D - 1/D}{2i} \cdot \mathfrak{J}_D{}'(0) = \frac{2i}{E - 1/E} \cdot \mathfrak{J}_D{}'(0) \\
\mathfrak{J}_F{}'(0) &= \frac{D + 1/D}{2} \cdot \mathfrak{J}_D{}'(0) = \frac{2}{F + 1/F} \cdot \mathfrak{J}_D{}'(0) \\
\mathfrak{J}_F{}'(0) &= \frac{-2}{F - 1/F} \cdot \mathfrak{J}_E{}'(0) = \frac{E + 1/E}{-2i} \cdot \mathfrak{J}_E{}'(0) \\
\wp_g{}''(0) &= \frac{2}{P + 1/P} \cdot (\mathfrak{J}_D{}'(0))^2
\end{aligned}
$$

(For the last line, insert $D^2 = (P+i)/(P-i)$ into $-D^2 \cdot (2i - P + 1/P) = D^2 \cdot (P-i)^2/P$.)

3.3 Specializations: Rectangular and Rhombic Tori.

3.3.1. Reflection symmetries. The tori with orientation-reversing symmetries are known as tori with complex conjugation. The ones that are quotients of $\mathbb{C}$ by rectangular lattices (basis $\{1, it\}$) are called *rectangular tori*, the ones with a lattice basis of equal length ($\{1, e^{i\varphi}\}$) are called *rhombic tori*. They are easy to distinguish: For the rectangular tori the axis of reflection in $\mathbb{C}$ is parallel to the edges of a rectangular fundamental domain and it projects to a fixed point set on the torus having *two* components; for the rhombic tori the axis of reflection in $\mathbb{C}$ is parallel to a diagonal of the rhombic fundamental domain and it projects to a fixed point set on the torus having *one* component. Now for a given elliptic function of degree two, only four of the reflections mentioned above have the property that they permute its branch points; either the axis of reflection passes through branch points or it passes through midpoints between branch points. Because the branch points—i.e. the fixed points of the 180^0 rotation by which we divide to get the degree two function — are permuted by the reflections of the torus, these orientation-reversing involutions pass to the sphere and we get further symmetries of our functions. We can determine these as Möbius-reflections in coordinate planes (i.e. $z \to \pm\bar{z}, z \to 1/\bar{z}$), because the fixed point set of the reflection passes through points at which we chose simple antipodal values of the function (namely, values in $\{0, \infty, \pm 1, \pm i\}$).

3.3.2. Rectangular Tori. The image under $\mathfrak{J}_D, \mathfrak{J}_E$ of the symmetry lines joining points with values $0, 1, \infty$ is the real line. It is therefore reasonable

to normalize $\mathfrak{J}_D{}'(0) = 1$,

because then $\mathfrak{J}_D, \mathfrak{J}_E, \mathfrak{J}_F$ map the real resp. the imaginary axis and the respectively parallel boundaries of the fundamental rectangle to the real resp. imaginary axis. The remaining symmetry lines are mapped to the unit circle, in particular $D \in \mathbb{S}^1$. We will mainly be interested in rhombic tori, but for illustrative purposes we first specialize our formulas to the rectangular case.
The branch values in the rectangular case (computed from D) are as follows:

$$D := e^{i\alpha};\ E = \frac{e^{i\alpha}-1}{e^{i\alpha}+1} = i\tan\alpha/2;\ F = \frac{\cos\alpha}{1+\sin\alpha};\ P = i \cdot \frac{e^{2i\alpha}+1}{e^{2i\alpha}-1} = \cot\alpha.$$

Each of the following differential equations (and also the equation between $\mathfrak{J}_D, \wp_g$) describe the torus in terms of its modular invariant $-\cot^2(\alpha)$:

$$\left(\frac{\mathfrak{J}_D{}'}{\mathfrak{J}_D}\right)^2 = (\mathfrak{J}_D{}^2 + \frac{1}{\mathfrak{J}_D{}^2} - 2\cos 2\alpha);$$

$$\frac{1}{4}\left(\frac{\wp_g{}'}{\wp_g}\right)^2 = -\frac{\sin 2\alpha}{2} \cdot (\wp_g - \frac{1}{\wp_g} - 2\cot 2\alpha) \quad = \quad \frac{1}{\mathfrak{J}_D{}^2}.$$

The *square torus* has the 45^0 diagonals as additional symmetry lines. Hence

$$\alpha = \pi/4, \quad P = 1, \quad \wp_g{}''(0) = \sin 2\alpha = 1.$$

In the figures below, the values indicated are values of $\wp_g$.

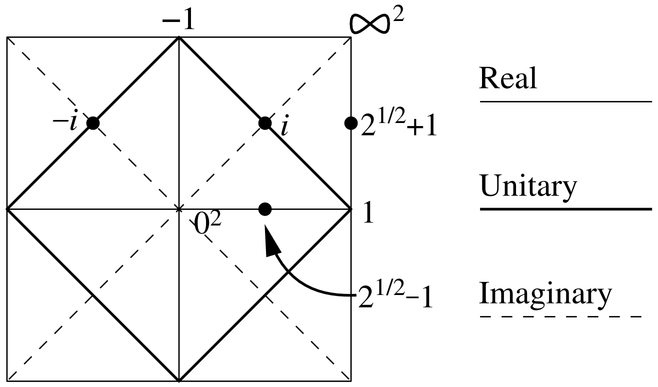

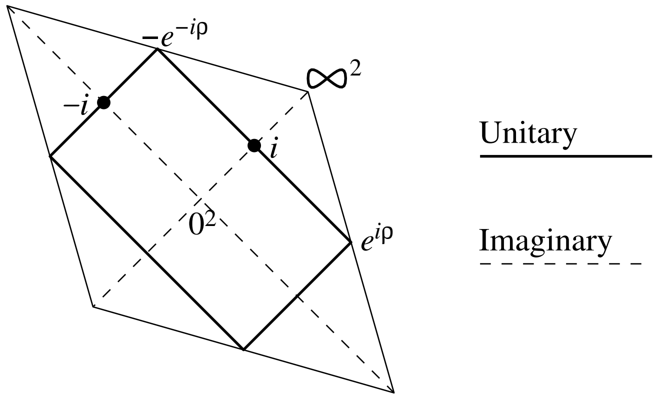

3.3.3. Rhombic Tori. We view these tori as deformations of the square torus which preserve the *diagonal* symmetries. Let μ denote reflection in one of the diagonals of the rhombic fundamental domain. Then we have

$$\overline{\mathfrak{J}_D \circ \mu} = i \cdot \mathfrak{J}_D, \quad \overline{\wp_g \circ \mu} = -\wp_g\ .$$

This says that on the diagonals we have $\mathfrak{J}_D \in e^{\pm i\pi/4} \cdot \mathbb{R}$, $\wp_g \in i \cdot \mathbb{R}$. The normalization $\mathfrak{J}_D{}'(0) = 1$ therefore implies that the diagonals of the rhombic fundamental domain point in the 45^0 directions—a reasonable rotational normalization. Furthermore we have for the branch values $\overline{D} = -i \cdot D, \overline{P} = 1/P$, and this gives us the branch value parametrization of rhombic tori via the following differential or functional equations:

$$
\begin{aligned}
D = R\cdot e^{i\pi/4},\quad P = e^{i\rho}, &\qquad \text{related via}\\
D^2 = iR^2 = \frac{P+i}{P-i} = \frac{i\cdot\cos\rho}{1-\sin\rho} &= i\cdot\cot(\pi/4-\rho/2);\\
\left(\frac{\mathfrak{J}_D{}'}{\mathfrak{J}_D}\right)^2 = (\mathfrak{J}_D{}^2 + \frac{1}{\mathfrak{J}_D{}^2} &- 2i\cdot\tan\rho);\\
\frac{1}{4}\left(\frac{\wp_g{}'}{\wp_g}\right)^2 = -\frac{1}{2\cos\rho}\cdot(\wp_g - \frac{1}{\wp_g} &- 2i\cdot\sin\rho) \quad = \frac{1}{\mathfrak{J}_D{}^2}.
\end{aligned}
$$

Our functions have more symmetries since we have two more reflections that permute the branch points. The above μ fixed the zeros of $\mathfrak{J}_D$ (where $\wp_g = 0,\infty$) and permuted the poles; now let ν be one of the reflections that fixes the poles of $\mathfrak{J}_D$ (where $\wp_g = e^{i\rho}, -e^{-i\rho}$) and permutes the zeros. Then:

$$
\begin{aligned}
&\overline{\wp_g\circ\nu} = \frac{1}{\wp_g}, \quad \text{i.e. } \wp_g \in \mathbb{S}^1 \text{ on the fixed point set of } \nu;\\
&\overline{\mathfrak{J}_D\circ\nu} = i\cdot\mathfrak{J}_D, \quad \text{i.e. } \mathfrak{J}_D \in e^{\pm i\pi/4}\cdot\mathbb{R} \text{ on the fixed point set of } \nu.
\end{aligned}
$$

For the other two functions $\mathfrak{J}_E, \mathfrak{J}_F$ we have relations such as $\overline{\mathfrak{J}_E\circ\mu} = -i\cdot\mathfrak{J}_F$, $\bar{E} = i\cdot F$, which we do not use.

4. Surfaces that lie in a continuous family of embedded examples with the genus-one helicoid

4.1 Scherk's doubly-periodic surface with a handle.

The lesson described in Section 2.3 allowed Karcher to add handles to Scherk's doubly-periodic surface, adding them not in each layer but in every *second* one only. The planar symmetry curves compatible with such an Ansatz cut the expected surface into four conformal rectangles, making the underlying Riemann surface a rectangular torus with four punctures. However we can assume in addition the existence of orthogonal horizontal straight lines at level 0 (as diagonals of the rectangles) on the surface. In other words, we have a diagonal symmetry of the underlying torus, which therefore must be *the* square torus.

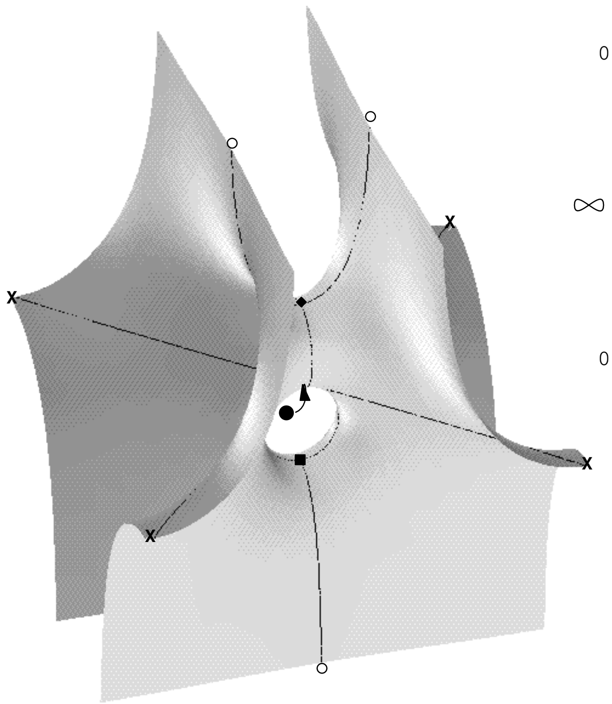

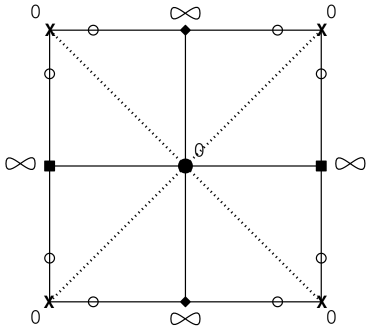

Basic piece of Scherk's doubly–periodic surface with handle, and parameterizing square torus. Values of Gauss map marked on the torus. Ends marked by ○.

As before, we now can see the Weierstrass data: The only vertical points of the Gauss map are at the vertices of the "four squares" (into which the symmetry curves cut the surface); the normals are alternatingly up and down. That is, the Gauss map of degree two is already determined, up to a constant real factor ρ (a phase factor being irrelevant). The four points with vertical normal are not punctures. Therefore we see from $ds = (|g| + 1/|g|) \cdot |dh|$ that dh has to have simple zeros at these four points. The four punctures, where dh has to have simple poles, are symmetric with respect to the straight line diagonals and they lie on the symmetry curves, i.e. on the boundary of the four tesselating squares. Now we know the poles of dh up to one real parameter R, and we know its zeros; i.e. we know our Weierstrass candidates. We have to choose $\rho(R)$ to make g horizontal at the punctures and then use R to solve the period problem. This time we wish to go into more detail because we are getting closer to the final example.

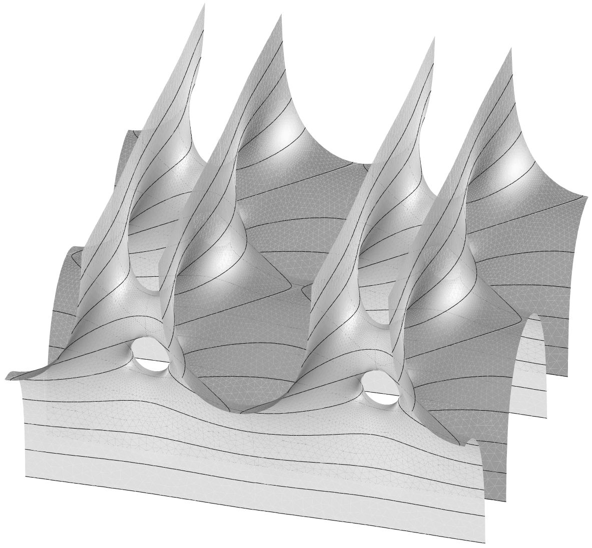

Figure 4
Scherk's doubly-periodic surface with a handle

4.2 Details for the Scherk surface with a handle.

4.2.1. Ansatz. With our explicit supply of elliptic functions we can now write formulae for the Weierstrass data. The square torus is given by each of the equations (3.3.2)

$$\frac{4}{\mathfrak{Z}_D{}^2} = -2(\wp_g - \frac{1}{\wp_g}) = \left(\frac{\wp_g{}'}{\wp_g}\right)^2.$$

The branch value parameters of $\wp_g$ and $\mathfrak{Z}_D$ are $P = 1,\ D = e^{i\pi/4}$. The Gauss map g and the differential dh, qualitatively described in section 4.1 (and recalling that a phase factor in the Gauss map only rotates the surface), are now given by:

$$g = \rho \cdot \mathfrak{Z}_D, \quad \rho \text{ a real parameter;}$$
$$dh = \left(\frac{\wp_g}{R} - \frac{R}{\wp_g}\right)^{-1} \cdot \frac{d\,\wp_g}{\wp_g}.$$

The poles of dh show that the punctures are where $\wp_g = \pm R$ or, using the equation of the torus, where $2/\mathfrak{Z}_D{}^2 = 1/R - R$. Since the Gauss map has to be unitary at the punctures we get from $g = \rho \cdot \mathfrak{Z}_D$:

$$\rho = \rho(R) = \sqrt{\frac{1}{2}(R - \frac{1}{R})}.$$

We mention that $|\,\mathfrak{Z}_D\,|$ and $|\,\wp_g\,|$ do not change their values if we reflect in the expected symmetry lines (the edges of the four tessalating squares and one of the diagonals of each square). These reflections are therefore Riemannian isometries of the metric $ds = (|g| + 1/|g|) \cdot |dh|$ of our Weierstrass data. Thus, we have realized the expected symmetry lines as geodesics (namely, fixed point sets of isometries).

4.2.2. Second fundamental form. Since the second fundamental form of a surface that is given by the Weierstrass integral (2.1.1) is (in a holomorphic coordinate system, so that tangent vectors are complex numbers) :

$$\mathrm{Re}\left(\frac{dg}{g} \cdot dh\right),$$

we see that $dh \cdot dg/g$ is real on the expected planar symmetry lines (resp. imaginary on the expected straight lines). These geodesics are therefore curvature (resp. asymptote) lines. That is, we have realized them as planar (resp. straight) symmetry lines on the minimal surface defined by the chosen data.

4.2.3. The period problem. The Weierstrass data do not have periods if the horizontal generator of the square torus is mapped to a closed planar curve in $\mathbb{R}^3$ (and, because of the diagonal symmetry, the same is then automatically true of the other generator). As noted at the end of Section 3, $\wp_g$ is real on this horizontal generator. This means we have to find R_0 such that:

$$\int_{\wp_g=0}^{\wp_g=1} \left(\frac{1}{\rho \cdot \mathfrak{Z}_D} - \rho \cdot \mathfrak{Z}_D\right) \cdot \left(\frac{\wp_g}{R_0} - \frac{R_0}{\wp_g}\right)^{-1} \frac{d\,\wp_g}{\wp_g} = 0.$$

Parametrizing along half the generator: $\wp_g = \tan(\varphi)$, $(0 \leq \varphi \leq \pi/4)$, we have

$$\frac{d\,\wp_g}{\wp_g} = \frac{2 \cdot d\varphi}{\sin 2\varphi}\,, \quad \mathfrak{Z}_D = \sqrt{\tan 2\varphi}\,.$$

Hence, we need $R = R_0$ such that

$$\int_0^{\pi/4} \left[\left(\sqrt{\frac{1}{2}(R - \frac{1}{R})\tan 2\varphi}\right)^{-1} - \sqrt{\frac{1}{2}(R - \frac{1}{R})\tan 2\varphi}\right] \cdot$$
$$\cdot\left(\frac{R}{\tan\varphi} - \frac{\tan\varphi}{R}\right)^{-1} \cdot \frac{2d\varphi}{\sin 2\varphi} = 0.$$

It is easy to check that the integral is positive for R close to 1 and negative for R very large, i.e. R_0 exists because of the intermediate value theorem. This is one of the simpler examples, among those cases where the period problem cannot be solved by symmetry arguments alone.

4.3 The genus one helicoid with translational symmetry.

The next development profited from the fact that Hoffman has been interested in the (frequently degenerate) limit surfaces in all families of embedded minimal surfaces that he came across [HW]. Previously, these limit surfaces were always simpler than the rest of the family and also already known. This was the first occasion where something new was found.

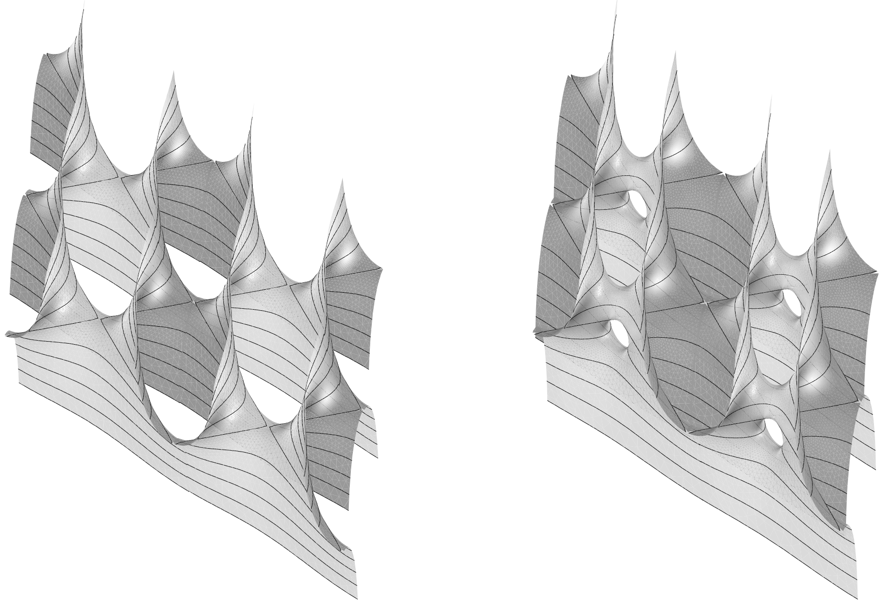

Figure 5

Perturbed Scherk's surface (left),
Perturbed Scherk's surface with handle (right)

Conceptually, it is easy to ask oneself whether the handle added to Scherk's surface in the previous section can survive a deformation similar to that of Scherk's doubly-periodic surface. In the same way as on Scherk's surface, we know that the vertical planar symmetry curves must disappear, but one could hope that the diagonal straight lines would persist. With the knowledge of the previous example, one is lead to generalize the Ansatz (4.2.1) to rhombic tori. One hopes that for each such torus - or at least for those close to the square torus - the complex parameter for the position of the puncture can be chosen so that it solves a period problem that is now two-dimensional. Very few such period problems have been solved to date. However, in this case Hoffman and Wei knew that the deformation of Scherk's doubly-periodic surface could be scaled in such a way that the limit surface was the helicoid. If the new deformation family did not degenerate too much, one could hope for a limit surface that would not be among those already known. This reward was worth the trouble and Wei succeeded in working out the family. Computer pictures showed that the convergence to the limit resembled that of the Scherk case. Thus a new limit surface appeared: a helicoid with one additional handle in each fundamental piece for the period translations!

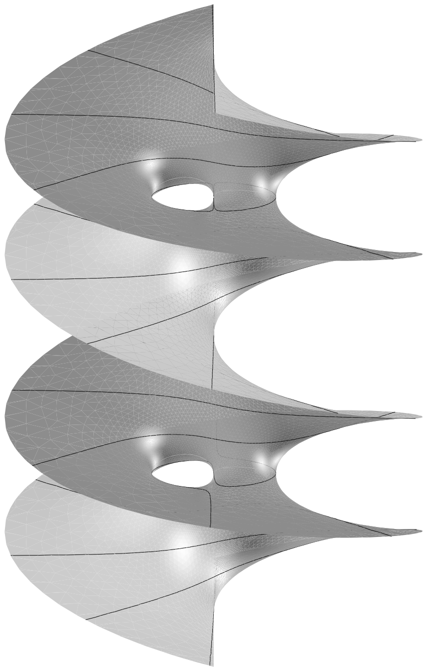

Figure 6
Genus one helicoid with translational symmetry

Once again, we are looking at a "qualitatively correct picture," and therefore can deduce from it the Weierstrass data of this limit surface. The problem simplifies further since these data have only a one-dimensional period problem. Here is the argument.

4.3.1. First we use the symmetries to specify the domain. The limit–surface, modulo translations, is a torus with two punctures. It carries a vertical straight line and 180^0 rotation around this line fixes no other points; therefore the torus is rhombic (3.3.1). The surface also contains (modulo translations) *two* parallel horizontal straight lines; on the torus these are given as one symmetry line separated into two components by two punctures. We choose the rhombic fundamental domain such that the straight lines correspond to the diagonals, and we call them the "vertical" and "horizontal" diagonal (corresponding to the vertical and horizontal lines on the surface). The 180^0 rotation around the surface normal at a point where the straight lines on the surface intersect (called a "symmetry" normal) maps the minimal surface to itself; on the quotient torus this is an orientation preserving involution with four fixed points, the 180^0 rotation r_P of section (3.1.4). Therefore, we view the quotient map $T^2 \to T^2/r_P$ as in (3.1.4) as the geometrically normalized Weierstrass $\wp$-function, $\wp_g$. We use this function to describe the torus analytically. We note the important fact that the two fixed points of r_P that are *not* on the vertical diagonal (i.e. the branch points of $\wp_g$ with finite branch values) are those points on the minimal surface where a symmetry normal intersects off the vertical line.

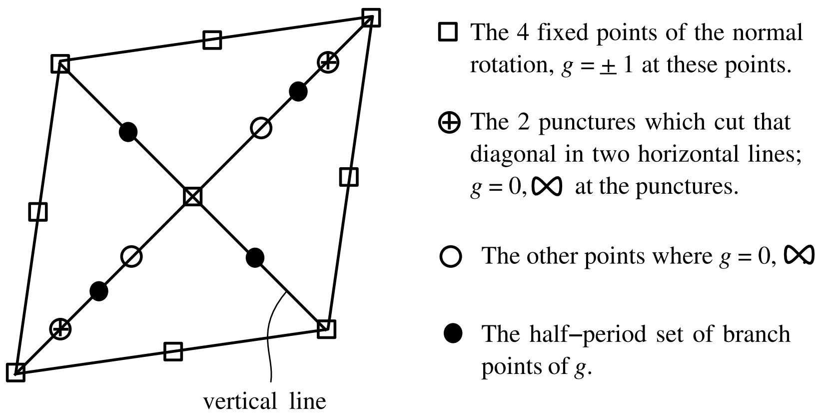

4.3.2. Next we determine the Gauss map from our qualitatively correct picture. It suggests that the Gauss map is of degree two. One zero and one pole are at the punctures on the horizontal diagonal (symmetric, of course, with respect to the midpoint). The other zero and pole also have to be on a symmetry line — because otherwise there would be more zeros and poles. This is only possible on the horizontal diagonal, since the Gauss map is unitary on the vertical diagonal. The branch points of the Gauss map are midpoints between the zeros (likewise between the poles). Therefore two branch points are on the horizontal diagonal. The four branch points of the degree two Gauss map are a half–period set which is *invariant* under the rotation r_P (since symmetries of a minimal surface permute the branch points of its Gauss map). The branch points of the Gauss map are therefore the quarter–points on the two diagonals of the rhombus. Looking back at (3.1.4) this implies that the Gauss map is a Möbius transformation of our function $\mathfrak{J}_D$. This Möbius transformation, together with the Gauss map, is determined up to *one* real parameter, since we want the zeros and poles to be on the horizontal diagonal. We will see shortly that the differential is determined by the Gauss map up to an irrelevant scaling factor. We have deduced on each rhombic torus a 1–parameter family of Weierstrass data candidates.

4.4 Details for the genus one helicoid with translational symmetry.

4.4.1. The rhombic tori. Recall, from Section 3.3.3, that the branch values of $\mathfrak{J}_D$ for a rhombic torus are $\pm D^{\pm 1}$, $D = R\cdot e^{i\pi/4}$, $R > 0$ and that the branch value P of $\wp_g$ is unitary, $P = e^{i\rho}$. We recall from (3.3.3) the equation of our rhombic torus as

$$\frac{2\cos\rho}{{\mathfrak{J}_D}^2} = -(\wp_g - {\wp_g}^{-1} - 2i\sin\rho).$$

4.4.2. The Gauss map. The following Möbius transformation of $\mathfrak{J}_D$ restates what we just said about the Gauss map; r is the real parameter which specifies the position of zeros and poles of g on the horizontal diagonal:

$$g = \frac{\mathfrak{J}_D - r\cdot e^{i\pi/4}}{\mathfrak{J}_D + r\cdot e^{i\pi/4}}.$$

4.4.3. The punctures. Next we state the properties of the differential dh; they determine it uniquely (depending on the parameters ρ, r of course). The differential has to have simple zeros at the two vertical points of g that are not the punctures and no other zeros; thus it has two poles, which have to be at the punctures. This already shows that dh is symmetric with respect to $0 \in T$. Finally dh has to be imaginary on the horizontal (sic!) diagonal (the Weierstrass representation shows: otherwise it could not be a level line). Recall that $\wp_g$ is imaginary on both diagonals and symmetric with respect to $0 \in T$. So we can write down dh in terms of $\wp_g$ if we denote the value of $\wp_g$ at the non-puncture points where $\mathfrak{Z}_D = \pm re^{i\pi/4}$ by $(\wp_g =)i\lambda$; at the punctures we then have $\wp_g = -1/(i\lambda)$ because we showed in section 3 that $\wp_g$ has the symmetry $\wp_g \to -1/\wp_g$ with respect to the branch points of $\mathfrak{Z}_D$. Of course we can express r in terms of λ or vice versa by using the equation of our torus:

$$\frac{2\cos\rho}{r^2} = \lambda + \lambda^{-1} - 2\sin\rho.$$

4.4.4. The differential. We denote by du the standard holomorphic form on the torus $T = \mathbb{C}/\Gamma$. We assume the normalization $du(1) = 1$, and therefore $du = d\wp_g / \wp_g'$. The Ansatz for dh can then be written as follows:

$$dh = e^{i\pi/4}\frac{\wp_g - i\lambda}{\wp_g - i\lambda^{-1}}du.$$

Again, we have deduced explicit Weierstrass data that define a two-parameter (ρ, λ)-family of minimal surfaces. For all of them, reflections in the diagonals are Riemannian isometries, i.e. these diagonals are geodesics. (They are also straight lines, namely geodesic asymptote lines, because the quadratic differential, whose real part is the second fundamental form, $dg/g \cdot dh$, is imaginary on the tangent vectors of the two diagonals.)

4.4.5. The period problem. Next let us formulate the period problem in a convenient way. 180^0 degree rotation around a symmetry normal of the minimal surface (namely the normal at the intersection of the vertical and a horizontal straight line) descends to the torus as an orientation-preserving involution, with four fixed points. With our choices, this is rotation around $0 \in T$ and the fixed points are the midpoint, "the" vertex of our fundamental rhombus, and the other two half-period points, i.e. the midpoints of the edges. Therefore, without computation, we have identified on the domain torus the two points where the normal symmetry line at height 0 meets the surface again. This identification allows a simple formulation of the period problem. Let I and II be the line segments in T connecting the half-period points as in (5.3.3).

4.4.6. The period condition for dh:

$$\mathrm{Re}\int_I dh = 0.$$

Symmetry then implies $\mathrm{Re}\int_{II} dh = 0$.

For each conformal parameter value $R^2 = 1/\tan(\pi/4 - \rho/2)$ this is a condition from which the parameter $\lambda(\rho)$ for the position of the punctures can be computed. (Computationally, it is in fact simpler to integrate the paths $I+II$ and $-I+II$, since $\wp_g$ has unitary values along these curves.)

4.4.7. Second period condition. Assume that the minimal surface is translated and rotated so that the symmetry normal which intersects the surface again (see 4.4.5) is the x_1-axis ($g = 1$ at the midpoint of the rhombus). Then (4.4.6) says that the other symmetry points (the half-period points on the torus) have $x_3 = 0$. The remaining period condition is that the x_2-coordinate also vanishes. Therefore we have from (2.2.1):

$$\mathrm{Re} \int_I i(\frac{1}{g} + g)dh = 0.$$

Because $\lambda(\rho)$ is determined by the period condition (4.4.6) for dh (4.4.4), this is a condition on the conformal parameter ρ that can readily be solved numerically. It is accessible to an intermediate value argument, albeit an argument more complicated than that in Section 4.2.3. We expect that the genus one helicoid with translational symmetry lies in a one parameter family of minimal surfaces, each one invariant under a screw-motion. Those that are translation-invariant can be expected to be limits of Scherk surfaces with fewer handles (the existence of which has not been proved).

4.4.8. Embeddedness. We should also mention that the Weierstrass representation cannot easily be used to decide whether a surface is merely immersed or in fact embedded. Sometimes a fundamental piece for the symmetry group can be shown to be a graph and this embedded piece is extended analytically by symmetries (rotations and reflections) to a complete embedded surface. Indeed, the most symmetric Scherk surface with a handle has fundamental pieces that are graphs, and its boundary curves are in pairwise orthogonal vertical symmetry planes, so that this surface is embedded. The Hoffman-Wei family includes this embedded surface and the ends (looking in $\mathbb{R}^3$ like parallel halfplanes) remain controlled under the deformation. Therefore —with more details to be published— all surfaces in the family, including the limit, are embedded.

5. The genus one helicoid.

5.1 Harold's challenge.

The final chapter starts with an amusing conversation. H. Rosenberg was visiting Bonn in the Spring of 1992. He was preparing a talk on embedded minimal surfaces with infinite isometry group, and he was also optimistic about approaching embedded minimal surfaces with at least two topological ends. But his ideas would not say anything about embedded minimal surfaces of finite topology with *just one end*. He said: "Hermann, I don't like this question to hang around. Why don't David and you sit down and construct such an example?"

— "Suggestions where to start looking?"
— "It is so easy for the helicoid, you just take the exponential map as Gauss map."
—"How many functions do you know with just one essential singularity on a torus?"
—"I think you are just lazy, you haven't even started to work on such an example."
—"How about taking the Hoffman-Wei example, fix one hole and slide the others to infinity?"
— "Do you really think you can do that and control the limit surface?"
— "Not now."
After this conversation things happened quickly. Two months later, with trans-Atlantic cooperation the new example was found.

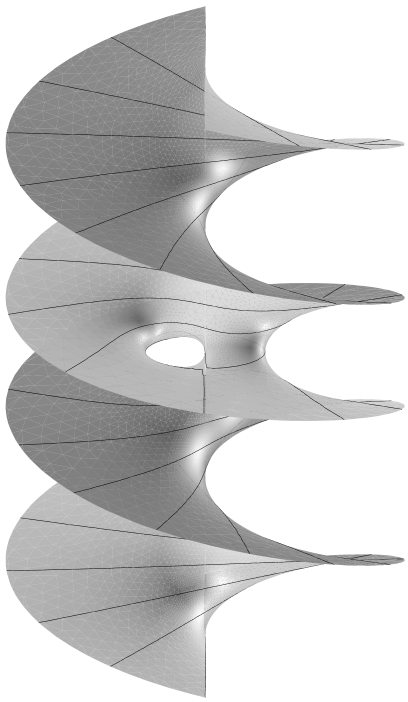

Figure 7

Genus one helicoid

5.2 The qualitatively correct picture.

5.2.1. The helicoid. The Weierstrass representation of the helicoid just alluded to is

$$g(z) := \exp(z) \quad , \quad dh := \frac{dg}{g} = dz \quad , \quad z \in \mathbb{C}.$$

The Mittag-Leffler theorem suggests to move the singularity to the origin as a first step in the construction of a doubly-periodic function, a Gauss map candidate. We get the helicoid in this form:

$$g(z) := \exp\left(\frac{1}{z}\right), \quad dh = \frac{dg}{g} = -\frac{dz}{z^2}, \quad z \in \mathbb{C} \cup \{\infty\} \setminus \{0\}.$$

Observe that the logarithmic differential dg/g becomes meromorphic with a *double pole*, just one order worse than the simple poles of logarithmic differentials of meromorphic functions. A strategy evolved: Do not go for the Gauss map immediately, work with the generalized Weierstrass representation where the differentials dg/g, dh are considered as the data, hope that these data are meromorphic for the desired example and deduce them under this meromorphicity assumption.

5.2.2. The initial strategy. How can one start to follow such a vague strategy? The helicoid suggests that dg/g and dh should have double poles at the puncture. The Riemannian metric $ds = (|g| + 1/|g|)|dh|$ shows that $|dh|$ cannot have other poles; so dh must have *two simple zeros* (resp., one double zero) and these have to be at simple (resp. double) vertical points of the Gauss map. The Hoffman-Wei helicoid suggests it is reasonable to assume one vertical and one horizontal straight line on the surface. This makes the underlying torus *rhombic* (3.3.1) because the fixed point set of the rotation about each of these lines has only one fixed point component. The two zeros of dh have to be on symmetry lines (because otherwise the symmetries would force four zeros) and they cannot be on the vertical line because the Gauss map needs to be vertical at the zeros of dh. Next, dg/g should have, as suggested by the helicoid, a double pole at the puncture. It should also have two simple poles with residues ± 1 at the two simple zeros of dh — so that g would have simple vertical points there to cancel the zeros of dh in the Riemannian metric. Because of the Riemannian metric, any further vertical point of g, not being compensated by a zero of dh, would lead to another puncture; therefore dg/g has no other poles. Hence there are four zeros, and it remains to place them symmetrically with respect to the diagonals. The Hoffman-Wei helicoid suggests, once more, placing two zeros on one diagonal (between the finite vertical points and the puncture) and the other two on the other diagonal.

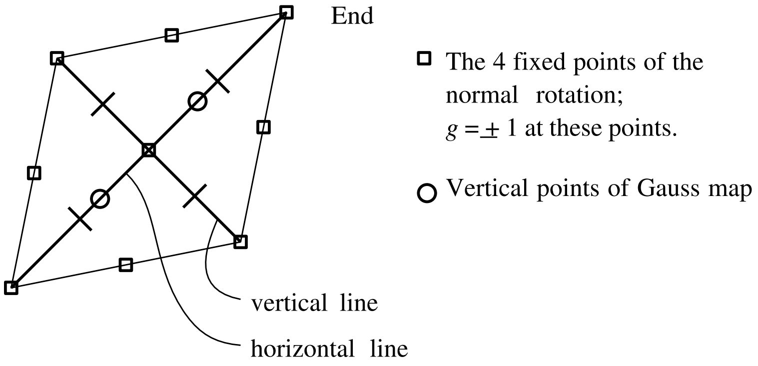

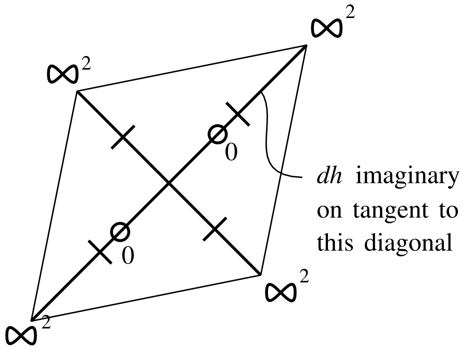

Zeros and poles of *dh*

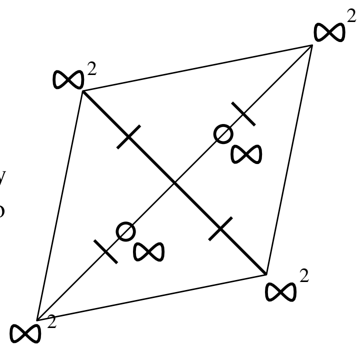

Poles of *dg/g*
Residue $\pm$ 1 at simple poles
(For placement of zeros, see (5.3.6))

5.3 First details for the genus one helicoid.

5.3.1. The rhombic tori. To get into more details we first decide to describe the family of rhombic tori by the differential equation of their geometrically normalized Weierstrass $\wp$-function $\wp_g$ with branch values $0, e^{i\rho}, \infty, -e^{-i\rho}$:

$$\left(\frac{\wp_g{}'}{\wp_g}\right)^2 = \frac{-2}{\cos\rho} \cdot \left(\wp_g - \frac{1}{\wp_g} - 2i\sin\rho\right).$$

5.3.2. The complex height differential. In terms of the function $\wp_g$ and the standard holomorphic differential form du, $du(1) = 1$ we can write down a differential form dh with:

- a double pole at the vertex of the rhombic fundamental domain;
- two simple zeros on one diagonal (we chose the $+45^0$ direction);
- and imaginary values on this diagonal, making it a level line of the third coordinate of the integral (2.1.1);

$$dh = e^{-i\pi/4} \cdot (\wp_g - i\epsilon) \cdot du = e^{-i\pi/4} \cdot (\wp_g - i\epsilon) \cdot (\frac{\wp_g{}'}{\wp_g})^{-1} \cdot \frac{d\,\wp_g}{\wp_g}.$$

Notice that the third condition, that the $+45^0$ diagonal is a level line, is satisfied since $\wp_g$ is imaginary on the diagonals of the rhombus (3.3.3).

5.3.3. The first period condition. Next we fix the parameter ϵ in the same way as we determined λ in (4.4.6) for the Hoffman-Wei helicoid: The rotation of the surface around the normal at the intersection of the two straight lines is an orientation-preserving involution of the torus, hence has four fixed points. On the torus, these are the half-period points, including the puncture. Therefore the normal rotation must fix two other points of the minimal surface. Obviously the normal has to intersect the surface in two more points, in addition to the intersection point of the straight lines. These points must be the images of the midpoints of the edges of the rhombic fundamental domain. Now let I and II be the segments from the midpoint of the rhombus to the labeled midpoints of its edges, as indicated in the diagram below. Then ϵ has to be chosen such that

$$\mathrm{Re}\int_I dh = 0\ ,\ \text{and by symmetry then also } \mathrm{Re}\int_{II} dh = 0.$$

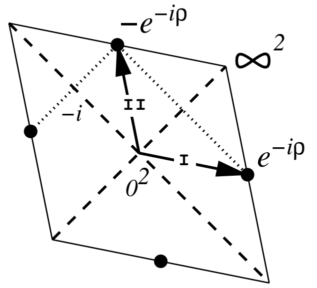

Values of $\wp_g$ are indicated in the diagram; $\wp_g$ is unitary on dotted lines connecting midpoints of edges.

This period condition simplifies if we observe that $\wp_g$ has unitary values on the straight segments between its branch points with values $e^{i\rho}, -e^{-i\rho}$. First, $\mathrm{Re}\int dh$ is 0 on the segment that cuts across the diagonal destined to be the vertical line, since the real part of $\wp_g$ is odd with respect to the midpoint $\wp_g = -i$ of this segment. Second, on the segment across the other, the "horizontal", diagonal we change variables to the unitary range of $\wp_g$. With $\wp_g = e^{i\varphi}$ we have $d\wp_g / \wp_g = i \cdot d\varphi$; with this and the differential equation (5.3.1) the above period conditon reduces to an explicit equation for $\epsilon(\rho)$, which we still call the

$$\text{“period condition for } dh \text{”:} \qquad \int_\rho^{\pi/2} \frac{\sin\varphi - \epsilon}{\sqrt{(\sin\varphi - \sin\rho)}} d\varphi = 0\ .$$

It can be written as:

$$\epsilon(\rho) = \sin\rho + \int_\rho^{\pi/2} \sqrt{(\sin\varphi - \sin\rho)}d\varphi \Big/ \int_\rho^{\pi/2} \frac{d\varphi}{\sqrt{(\sin\varphi - \sin\rho)}}.$$

5.3.4. The control of ϵ. We will need a little information about ϵ to even write down the Ansatz for dg/g. Some more precise information is required to show that the period conditions for dg/g can always be satisfied (with parameter values in the Ansatz that are compatible with our qualitative picture). For the final intermediate value proof we will need:

- quite precise information about $\epsilon = \epsilon(\rho)$ as ρ approaches $+\pi/2$;
- the existence of a $\rho_+ < 0$ such that $\epsilon(\rho) > 0$ for $\rho \in (\rho_+, \pi/2)$;
- the existence of a $\rho_- > -\pi/2$ such that $\epsilon(\rho_-) < 0$.

All this is supplied by the following

LEMMA.

(i) For $-\pi/6 \le \rho < \pi/2$, the following equivalent estimates ($<^*$) hold, while for $0 \le \rho < \pi/2$, the other equivalent estimates ($<$) hold:

$$\begin{aligned}
\frac{1}{3}(1-\sin\rho) &<^* \ \epsilon(\rho) - \sin\rho \ < \frac{2}{3}(1-\sin\rho),\\
\frac{1}{3}(1-\sin\rho) &< \ 1-\epsilon(\rho) \ <^* \frac{2}{3}(1-\sin\rho),\\
0 \le \frac{1}{3}(2\sin\rho+1) &<^* \quad \epsilon(\rho) \quad < \frac{1}{3}(\sin\rho+2) < 1.
\end{aligned}$$

(ii) For $-\pi/2 < \rho < \pi/2$, we have:

$$\epsilon(\rho) < \sin\rho + \frac{1}{3}\cdot(\pi/2-\rho);$$

consequently,

$$\cos\rho_- = \frac{1}{3}, \quad \epsilon(\rho_-) \le -0.008 < 0.$$

PROOF. We estimate the quotient of the integrals in (5.3.3). The trivial bound

$$\sin\varphi - \sin\rho \le \varphi - \rho$$

can be used in the numerator and denominator to get part (ii):

$$\int_\rho^{\pi/2} \sqrt{(\sin\varphi-\sin\rho)}d\varphi \ \le \int_\rho^{\pi/2} \sqrt{(\varphi-\rho)}d\varphi \ = \frac{2}{3}(\pi/2-\rho)^{3/2}$$

$$\int_\rho^{\pi/2} \frac{d\varphi}{\sqrt{(\sin\varphi-\sin\rho)}} \ \ge \int_\rho^{\pi/2} \frac{d\varphi}{\sqrt{(\varphi-\rho)}} \ = 2(\pi/2-\rho)^{1/2}.$$

The minimum of $\sin\rho + \frac{1}{3}(\pi/2-\rho)$ in $(-\pi/2, 0)$ is obtained when $\cos\rho = 1/3$, $\sin\rho = -\sqrt{8/9}$; the value of ϵ at this ρ is $\le -0.008 < 0$.
In order to establish estimate(i) we use the following bounds:
For $0 \le \rho < \pi/2, \sin\varphi$ is below its tangent in $\rho < \varphi < \pi/2$:

$$\sin\varphi - \sin\rho \ < \ \cos\rho\cdot(\varphi-\rho);$$

for $-\pi/6 \le \rho < \pi/2$, then $\sin\varphi$ is above its secant in $\rho < \varphi < \pi/2$:

$$(1-\sin\rho)\cdot\frac{\varphi-\rho}{\pi/2-\rho} \ <^* \ \sin\varphi - \sin\rho.$$

As before, these inequalities are inserted in the integrals and explicit integration gives us estimates which we will need again, the following

5.3.5. Integral bounds:

$$\sqrt{1-\sin\rho}\cdot\frac{2}{3}(\pi/2-\rho) <^* \int_{\rho}^{\pi/2}\sqrt{(\sin\varphi-\sin\rho)}d\varphi$$

$$< \sqrt{\cos\rho}\cdot\frac{2}{3}(\pi/2-\rho)^{3/2};$$

$$2 \le \frac{2}{\sqrt{\cos\rho}}\cdot(\pi/2-\rho)^{1/2} < \int_{\rho}^{\pi/2}\frac{d\varphi}{\sqrt{(\sin\varphi-\sin\rho)}}$$

$$<^* \frac{2}{\sqrt{1-\sin\rho}}\cdot(\pi/2-\rho) \le 4.$$

These imply the inequalities ($<^*$) in the Lemma, the others follow from the simplification

$$\frac{1}{3}\cos\rho\cdot(\pi/2-\rho) = \frac{4}{3}\sin\frac{\pi/2-\rho}{2}\cdot\cos\frac{\pi/2-\rho}{2}\cdot\frac{\pi/2-\rho}{2}$$

$$\le \frac{4}{3}(\sin\frac{\pi/2-\rho}{2})^2 = \frac{2}{3}(1-\sin\rho).$$

5.3.6. The Ansatz for dg/g. So far, we have a unique candidate for dh on each rhombic torus, but we are not interested in those tori for which $\epsilon(\rho)\le 0$. Next we make an Ansatz for dg/g which expresses in formulas what we explained in (5.2.2). Namely we want dg/g to have:

- two simple poles with residues ± 1 where $\wp_g = i\epsilon$ (these will give us the vertical points of g on the horizontal line);
- a double pole at the vertex of the rhombic fundamental domain (which will give us an essential singularity of g very much like that of $\exp(1/z)$);
- four zeros (forced by the four poles) at the points where $\wp_g = i\cdot r,\ \wp_g = i\cdot E$ (which will give us two branch points of g on each straight line).

As before, we want to make use of the symmetries of $\wp_g$ and therefore express the holomorphic differential du as in (4.4.4):

$$du = \left(\frac{\wp_g{}'}{\wp_g}\right)^{-1}\cdot\frac{d\,\wp_g}{\wp_g},\quad du(1)=1.$$

Recall that in a holomorphic coordinate system, tangent vectors are complex numbers; therefore $du(1)=1$ means that the holomorphic differential on the torus is normalized to have the value 1 on the unit tangent vector of the real axis. With this in mind we are able to write:

$$\frac{dg}{g} =$$

$$e^{i\pi/4}\cdot\frac{(\wp_g-ir)}{\epsilon-r}\cdot\frac{(\wp_g-iE)}{\epsilon-E}\cdot\frac{\epsilon}{\wp_g}\cdot\left[\sqrt{\frac{2}{\cos\rho}(\epsilon+\frac{1}{\epsilon}-2\sin\rho)}\,\right]\left(\frac{\wp_g{}'}{\wp_g}\right)^{-1}\cdot\frac{d\,\wp_g}{\wp_g-i\epsilon}.$$

We recall that $\wp_g$ is imaginary on the diagonals of the rhombus, which have the $\pm 45^0$ directions, and $e^{i\pi/4}du(e^{\pm i\pi/4}) = i$ resp., 1. Therefore, we see that the phase factor $e^{i\pi/4}$ in the Ansatz is adjusted to make dg/g *real* on the tangent vector of the "horizontal" diagonal (the one which corresponds to the horizontal line on the surface and which has the vertical points at $\wp_g = i\epsilon$) and *imaginary* on the other, the "vertical" diagonal, where we wish the Gauss map to be unitary. The square-root factor makes the residue at $\wp_g = i\epsilon$ equal to ± 1. Observe that this is very close to the data of the Hoffman-Wei helicoid: One only has to move the two simple poles of dg/g which correspond to their punctures so that they merge to our double pole at the vertex of the rhombic fundamental domain. Of course, even a deformation in that direction is impossible with a meromorphic Gauss map, but on the level of differential forms we gain this flexibility.
Technically we will find it convenient to rewrite dg/g in terms of

$$X := (E-\epsilon) + (r-\epsilon), \quad Y := (E-\epsilon)\cdot(\epsilon - r)$$

as follows:

$$\frac{dg}{g} =$$

$$-\epsilon\left[\sqrt{\frac{2}{\cos\rho}(\epsilon + \frac{1}{\epsilon} - 2\sin\rho)}\,\right]\cdot\left(\frac{1}{\wp_g - i\epsilon} - \frac{(\wp_g - i(X+\epsilon))}{Y}\right)e^{i\pi/4}\left(\frac{\wp_g{}'}{\wp_g}\right)^{-1}\frac{d\,\wp_g}{\wp_g}.$$

5.3.7. The period condition for dg/g. The next step is the determination of the parameters r, E, or more conveniently X, Y in such a way that $g = \exp(\int dg/g)$ is a well-defined function on the torus. We translate the minimal surface so that the intersection point of the straight lines is $0 \in \mathbb{R}^3$ and rotate so that the Gauss map has the value $g = 1$ there, at the midpoint of the rhombic fundamental domain. We have already explained that 180^0 rotation around this ($g = 1$)-normal (the x_1-axis) is an isometry of the minimal surface; it induces an orientation-preserving involution of the torus. Its fixed points are the half-period points, the branch points of $\wp_g$. Therefore this symmetry normal must intersect the minimal surface in two more points, which are, on the torus, the points where $\wp_g$ is equal to $P = e^{i\rho}$ or to $-1/P = -e^{-i\rho}$. Again we denote the straight segments from the midpoint of the rhombus to the midpoints of the edges I, II, see diagram (5.3.3). The integrals of dg/g along these paths are (because of the rotational symmetry around the straight lines) equal up to sign; by joining the endpoints of I, II we get two pairs of isosceles triangles. The ones with a point where $\wp_g = +i$ on their baseline contain one of the points where $\wp_g = i\epsilon$, i.e., where the residue of dg/g is ± 1, in their interior (since $\epsilon < 1$); the other triangles (baseline orthogonal to the "vertical" diagonal) contain no singularity of dg/g inside. This leaves only the possibility that the integral of dg/g along the paths I, II is $\pm i\pi$. In particular, the Gauss map has the opposite value $g = -1$ at the other intersections with the x_1-axis—in agreement with the qualitative picture suggested by the Hoffman-Wei helicoid. So we arrived at a convenient formulation of the

$$\text{"period condition for } dg/g\text{ ":} \qquad \int_{I,II}\frac{dg}{g} = \pm\pi i, \text{ or } \int_{I\pm II}\frac{dg}{g} = 0.$$

Again it is helpful to use the fact that $\wp_g$ is unitary on the straight segments $I \pm II$ between the branch points, where $\wp_g = e^{i\rho}, -e^{-i\rho}$. Along the path orthogonal to the "vertical diagonal," $e^{i\pi/4}du$ is imaginary on tangent vectors and—as follows from (3.3.3)—, $\operatorname{Re}\wp_g$ is odd and $\operatorname{Im}\wp_g$ is even with respect to the midpoint (where $\wp_g = -i$). It follows that the integral of the proposed dg/g is real along this path; along the other path, $\wp_g$ has the same symmetries, but $e^{i\pi/4}du$ gives real values, making the integral of dg/g imaginary. This shows that the symmetries help us to satisfy two complex period conditions by adjusting two real parameters. As before, we use $\wp_g$ as coordinate map and do the integration in the range of this chart. That is, we substitute $\wp_g = e^{i\varphi}, d\wp_g/\wp_g = i \cdot d\varphi$ in our Ansatz for dg/g, use the differential equation (5.3.1) to express $\wp_g'/\wp_g$ and then plug the result into the last version of the period condition above (integration along $I \pm II$). Finally, we take the real (resp. imaginary) part, which is not automatically zero, and end up with the following *linear system* for X, Y, which expresses our period conditions for dg/g. The zero in the first equation is nothing but the definition of ϵ.

$$0 = A_1 \cdot X \;+\; B_1 \cdot Y, \qquad \text{namely:}$$

$$0 = \int_\rho^{\pi/2} \frac{d\varphi}{\sqrt{(\sin\varphi - \sin\rho)}} \cdot X + \int_\rho^{\pi/2} \frac{\sin\varphi - \epsilon}{1 + \epsilon^2 - 2\epsilon\sin\varphi} \cdot \frac{d\varphi}{\sqrt{(\sin\varphi - \sin\rho)}} \cdot Y$$

$$C_2 = -A_2 \cdot X \;+\; B_2 \cdot Y, \qquad \text{namely:}$$

$$+\int_{-\rho}^{\pi/2} \frac{\sin\varphi + \epsilon}{\sqrt{(\sin\varphi + \sin\rho)}}\, d\varphi$$

$$= -\int_{-\rho}^{\pi/2} \frac{d\varphi}{\sqrt{(\sin\varphi + \sin\rho)}} \cdot X + \int_{-\rho}^{\pi/2} \frac{\sin\varphi + \epsilon}{1 + \epsilon^2 + 2\epsilon\sin\varphi} \cdot \frac{d\varphi}{\sqrt{(\sin\varphi + \sin\rho)}} \cdot Y\ .$$

5.3.8. First consequences of the period condition for dg/g. Clearly we have

$$0 \;<\; A_1, C_2, A_2, B_2.$$

CLAIM. We also have: $\quad 0 \;<\; B_1.$

PROOF. By definition of ϵ we have first that the function

$$f(\varphi) := \frac{\sin\varphi - \epsilon}{\sqrt{\sin\varphi - \sin\rho}} \quad \text{satisfies} \quad \int_\rho^{\pi/2} f(\varphi)d\varphi \;=\; 0,$$

and $f < 0$ to the left, $f > 0$ to the right of its simple zero at $\varphi_\epsilon, \sin\varphi_\epsilon = \epsilon$. Second, the function

$$g(\varphi) := 1/(1 + \epsilon^2 - 2\epsilon\sin\varphi)$$

is positive and increasing in the interval $(\rho, \pi/2)$. Together this proves the claim:

$$B_1 = \int_{\rho}^{\pi/2} f(\varphi) \cdot g(\varphi) \cdot d\varphi \;=\; \int_{\rho}^{\pi/2} (f(\varphi) - f(\varphi_\epsilon)) \cdot (g(\varphi) - g(\varphi_\epsilon)) d\varphi \;>\; 0.$$

QED

An immediate consequence is that our linear system *always* has a solution and that the values are in agreement with our qualitative picture:

$$Y > 0, X < 0.$$

Hence (solving $t^2 - X \cdot t - Y = 0$) we have established that

$$r - \epsilon < 0 < E - \epsilon < \epsilon - r.$$

We draw one more immediate conclusion:
Let ρ decrease so that $\epsilon(\rho) \to 0$; because of (5.3.4) ρ stays bounded away from $-\pi/2$. Therefore one can easily take the limit $\epsilon \to 0$ in the coefficients of our linear system. We obtain $B_1 \to 0, A_2/C_2 \to 1$, while A_1 stays bounded away from 0. So we get

$$\epsilon \to 0 \quad \text{implies} \quad X \to 0,\ Y \to 1,\ r \to -1,\ E \to +1.$$

This surprising simplification is responsible for one half of the final intermediate value argument.

5.3.9. The one-parameter family of candidates. We summarize what we have achieved. The previous derivations lead us to *define* dh by (5.3.2) and dg/g by (5.3.6); then the single period condition for dh and the two period conditions for dg/g can, for all $\rho \in (\rho_0, \pi/2)$, be solved uniquely where ρ_0 satisfies $\epsilon(\rho_0) = 0$, and is estimated by (5.3.4) as $-\frac{\pi}{2} < \rho_- < \rho_0 < \rho_+ < -\frac{\pi}{6}$. With these choices of r, E or X, Y the definition

$$g := \exp \int_0 \frac{dg}{g}$$

gives a well-defined function on each of our rhombic tori (restricted by $\epsilon(\rho) > 0$). (These candidates for the Gauss map of the genus one helicoid are special choices of Baker-Akhiezer functions, as we now know.) Hence, on each such torus we have arrived at a unique Weierstrass data candidate $\{g, dh\}$ for the surface we wish to construct!
The minimal surface family *defined* by these Weierstrass data has, because of our careful choice of parameters, the following properties:

- the diagonals of the rhombic fundamental domain are a horizontal and a vertical straight line on the surface;
- the Gauss map has an essential singularity like that of $\exp(1/z)$ at the vertex of the rhombus;
- the Gauss map has value $g = +1$ at the midpoint, and value $g = -1$ at the remaining two half-period points (recall that the puncture is at the fourth half-period point, the vertex of the rhombus);

- these three half-period points are on the same level. $x_3 = 0$, where x_3 is the height function $x_3 := \mathrm{Re}\int_0 dh$;
- 180^0 rotation around the normal at the origin (where $g = 1$) is a symmetry of the surface for all ρ (with $\epsilon(\rho) > 0$).

Therefore we have almost achieved our goal. For the existence part only one problem remains: The two half-period points with $g = -1$ have to be points that, as points on the minimal surface, lie not only on the same level as the origin (which they do because of 5.3.3), but that in fact lie on the x_1-axis (which is the symmetry normal at the origin). We solve this problem with an intermediate value argument: The sign of the x_2-coordinate of those half-period points is different near the two limit situations (i) $\epsilon(\rho) \to 0$, (ii) $\rho \to \pi/2$. To prove this requires two things: precise estimates for Y; a judicious choice of paths of integration to the half-period points on the torus, along which our other estimates are sharp enough to help to determine the sign of the x_2 coordinate in the limit situations. Numerically, we could find the solution long before we could do the estimates.
We would like to establish embeddedness by proving the existence of the continuous family of minimal surfaces (mentioned earlier) that joins the new surface to an embedded one. For this to work, we must control their behavior at infinity so well that they all have to be embedded. This needs further study—at the moment only the pictures show that the new surface is embedded. We now return to the existence proof.

5.4 Estimates for the linear system.

5.4.1. The aim.

At first the intermediate value proof attempt looked discouraging because it seemed to require precise information about the parameters ϵ, X, Y of our Weierstrass data in two different ranges of the conformal parameter ρ. We have already explained in (5.3.8) that as $\epsilon \to 0$, the other parameters converge to *known* values and no further estimates will be needed for that part of the proof. The amount of work we have to do is again reduced because we found a path on the torus along which a good lower bound for Y is enough to finish the argument. The aim of this section is to prove the sufficient lower bound:

$$\frac{\pi}{4} \le \rho < \frac{\pi}{2} \quad \text{implies } \frac{1}{23} \cdot (1 - \sin\rho)^{5/8} \ \le \ Y(\rho).$$

Our strategy will be to substitute the first equation (5.3.7), namely
$-X = B_1/A_1 \cdot Y$, into the second equation and estimate towards lower bounds for Y.

5.4.2. The first three estimates:

$$2 \le A_1\ , \quad \frac{B_2}{A_2} \le \frac{1}{2\epsilon}\ , \quad 1 \le C_2.$$

Proof. First, $2 \le A_1 \le 4$ has already been obtained in (5.3.5). Second, to estimate $2\epsilon \cdot B_2/A_2$ it is enough to increase the numerator of the integrand of B_2, using $0 < \epsilon < 1$, a little:

$$2\epsilon \cdot (\sin\varphi + \epsilon) \leq 1 + \epsilon^2 + 2\epsilon \sin\varphi$$

to get the *same* integrand as for A_2. Hence $2\epsilon \cdot B_2/A_2 \leq 1$.

And to estimate C_2 we first use $\sin\rho \leq \epsilon$ (5.3.4) and then estimate trivially (assuming always in this section that $\pi/4 \leq \rho$):

$$C_2 := \int_{-\rho}^{\pi/2} \frac{\sin\varphi + \epsilon}{\sqrt{\sin\varphi + \sin\rho}} d\varphi \;\geq\; \int_{-\rho}^{\pi/2} \sqrt{\sin\varphi + \sin\rho}\, d\varphi \;\geq\; \int_{0}^{\pi/2} \sqrt{\sin\rho}\, d\varphi$$

$$\geq\; \frac{\pi}{2}\sqrt{\sin\pi/4} \;\geq 1.3$$

5.4.3. The upper bound:

$$A_2 \leq 2 + 5 \cdot (\cos\rho)^{-1/4}.$$

Proof. The integral for positive φ is easy:

$$\int_{0}^{\pi/2} \frac{d\varphi}{\sqrt{\sin\varphi + \sin\rho}} \;\leq\; \frac{\pi}{2\sqrt{\sin\rho}} < 2\ .$$

For the other part we need the following estimate. For $0 \leq \alpha \leq \pi/4$ and all $x \in (\alpha, \pi/2)$:

$$\cos x \leq \cos\alpha - \sin\alpha \cdot (x - \alpha) - \frac{\cos\alpha}{6} \cdot (x - \alpha)^2.$$

This is true at $x = \alpha$ and follows for all $x \in (\alpha, \pi/2)$ if we have for the derivative

$$-\sin x \leq -\sin\alpha - \cos\alpha (x - \alpha)/3;$$

and indeed

$$\frac{\sin x - \sin\alpha}{x - \alpha} \geq \frac{1 - \sin\alpha}{\pi/2 - \alpha} \geq \frac{1 - \sin\alpha}{\sin(\pi/2 - \alpha) \cdot \pi/2} = \frac{\cos\alpha}{(1 + \sin\alpha) \cdot \pi/2} \;>\; \frac{\cos\alpha}{3}.$$

We will use this estimate in the following form:

$$\pi/4 \leq \rho < \pi/2,\ \ -\rho \leq \varphi \leq 0 \quad \text{implies}\ \cos\rho \cdot (\varphi + \rho) + \frac{\sin\rho}{6}(\varphi + \rho)^2 \leq \sin\varphi + \sin\rho.$$

Hence

$$\int_{-\rho}^{0} \frac{d\varphi}{\sqrt{\sin\varphi + \sin\rho}} \;\leq \int_{0}^{\rho} \frac{dt}{\sqrt{t\cos\rho + t^2 \sin(\rho)/6}} \;\leq \int_{0}^{\rho} \frac{dt}{\sqrt{2\sqrt{t^3 \cos(\rho)\sin(\rho)/6}}}$$

$$= \sqrt{\frac{\sqrt{6}}{2}} \cdot \frac{4}{(\cos\rho)^{1/4}} \cdot \Big(\frac{\rho}{\sin\rho}\Big)^{1/4} \;\leq\; 5(\cos\rho)^{-1/4},$$

which gives the claimed bound for A_2.

5.4.4. The final estimate for Y. So far we have derived from the linear system the following inequalities

$$0 < -2 \cdot X \le B_1 \cdot Y$$

$$\frac{(1-\sin\rho)^{1/8}}{7} \le \frac{(\cos\rho)^{1/4}}{5+2(\cos\rho)^{1/4}} \le -X + \frac{1}{2\epsilon}\cdot Y.$$

The missing information about B_1 is supplied by the

Claim:

$$\frac{1}{2}B_1 \le 2.8\cdot(1-\sin\rho)^{-1/2},$$

from which we conclude the aim of this section (5.4) as follows

$$\frac{(1-\sin\rho)^{1/8}}{7} \le (2.8\cdot(1-\sin\rho)^{-1/2} + \frac{1}{2\epsilon})\cdot Y \le 3.2\cdot(1-\sin\rho)^{-1/2}\cdot Y,$$

or

$$\frac{1}{22.4}(1-\sin\rho)^{5/8} \le Y.$$

Proof of the Claim. It is sufficient to estimate only the positive part of the integrand of B_1. First we get rid of some factors that do not matter, by using bounds for ϵ derived in (5.3.4):

$$\sqrt{\sin\varphi-\sin\rho} \le \sqrt{1-\sin\rho}, \quad \sin\varphi-\epsilon \le 1-\epsilon \le \frac{2}{3}(1-\sin\rho),$$

$$\frac{2\epsilon}{1+\epsilon^2-2\epsilon\sin\rho} \le \frac{1}{1-\sin\rho}.$$

Then, with $\sin\varphi_\epsilon = \epsilon$, the integral simplifies to

$$\frac{1}{2}B_1 \le \frac{\sqrt{1-\sin\rho}}{3}\cdot\int_{\varphi_\epsilon}^{\pi/2}\frac{d\varphi}{1+\epsilon^2-2\epsilon\sin\varphi}.$$

Again we replace $\sin\varphi$ by a Taylor expansion and use Schwarz inequality to get an explicitly integrable term. Under the assumptions

$$\pi/4 \le \rho \le \varphi_\epsilon, \quad \varphi_\epsilon \le \varphi \le \pi/2$$

we have (again using (5.3.4))

$$\sin\varphi \le 1-(\pi/2-\varphi)^2/2.2 \text{ and } 0.8 \le \epsilon.$$

We insert this in the integrand and also use that $0 \le a, b$ implies $1/(a^2+b^2) \le 2/(a+b)^2$ to get

$$\frac{1}{(1-\epsilon)^2+2\epsilon(1-\sin\varphi)} \le \frac{2.2}{2.2(1-\epsilon)^2+2\epsilon(\pi/2-\varphi)^2} \le \frac{2.8}{((1-\epsilon)+(\pi/2-\varphi))^2},$$

$$\int_{\varphi_\epsilon}^{\pi/2}\frac{d\varphi}{(1-\epsilon+\pi/2-\varphi)^2} = \frac{1}{1-\epsilon+\pi/2-\varphi}\Big|_{\varphi_\epsilon}^{\pi/2} \le \frac{1}{1-\epsilon} \le \frac{3}{1-\sin\rho}.$$

Insertion of these two lines in the last expression bounding B_1 proves the claim.

QED

5.5 The solution of the remaining period problem.

5.5.1. What can still go wrong?
The summary in (5.3.9) emphasized the fact that we have, at this point, produced a one-parameter family of possible candidates, parametrized by a conformal parameter ρ, where $e^{i\rho}, -e^{-i\rho}$ are the branch values $\neq 0, \infty$ of $\wp_g$ on a rhombic torus. For each such torus we have a *unique* candidate for dh (5.3.2, 5.3.3) and g (5.3.6 - 5.3.8), which have the five properties listed in (5.3.9). These candidates have symmetry normals at the three finite valued branch points of $\wp_g$, $\wp_g = 0, e^{i\rho}, -e^{-i\rho}$, i.e. 180^0 rotation around the normals at these points is a symmetry of the minimal surface (defined by our $dh,\ g$). These points lie in the (x_1, x_2)-plane by construction; but if they are not on one single normal line (here the x_1-axis), then composition of these normal rotations produces nontrivial translational symmetries, the so called periods. Our computer calculations showed that there is a choice of ρ, for which these periods vanish, so that the Weierstrass integral (2.1.1) defines a well defined map from the punctured torus (determined by ρ) into $\mathbb{R}^3$. It remains to *prove* this fact.

5.5.2. Outline of the intermediate value argument.
We will show the existence of the desired ρ by applying the intermediate value theorem to the second coordinate function of the minimal surface at the branch point $\wp_g = e^{i\rho}$, which is a continuous function of ρ. The one point $\wp_g = e^{i\rho}$ on the torus has two representatives in the rhombic fundamental domain; to get a well defined function we restrict the Weierstrass integral to a simply connected part of the punctured torus. We take one half of the fundamental rhombus (without the puncture), the half to the *right* of the "vertical" diagonal. Recall that the vertical diagonal corresponds to the vertical line on the minimal surface; it has the two points $\wp_g = -i$ on it. The "horizontal" diagonal has the points $\wp_g = i$ on it. Now we have in the *right half of the rhombus* two paths from $\wp_g = 0$ to $\wp_g = e^{i\rho}$ (and also two paths to $\wp_g = -e^{-i\rho}$) which are distinguished because $\wp_g$ is first imaginary and then unitary along them:

a) For ρ near $\pi/2$ it is better to integrate first from $\wp_g = 0$ to $\wp_g = i$ along the horizontal diagonal and then from $\wp_g = i$ to $\wp_g = e^{i\rho}$ (or $-e^{-i\rho}$) along the -45^0 segment, because the following is proved in (5.6): The length of the horizontal line from $\wp_g = 0$ to $\wp_g = i$ stays bounded away from 0, while the length of the segment from $\wp_g = i$ to $\wp_g = e^{i\rho}$ can be bounded by const$\cdot(\pi/2 - \rho)$. This means that the Weierstrass integral maps the branch points $\wp_g = e^{i\rho}, -e^{-i\rho}$ into the (x_1, x_2)-plane on the *same* side of the x_1-axis as the horizontal half-line (from the right half of the rhombus), for ρ close to $\pi/2$.

b) For ρ in a range where $\epsilon(\rho) > 0$ is very small it is better to integrate first along the vertical diagonal from $\wp_g = 0$ to $\wp_g = -i$ and then from $\wp_g = -i$ to $\wp_g = e^{i\rho}$ (always to the right of the vertical diagonal). Along the vertical line the x_2-coordinate remains zero. We prove in (5.7) that near the limit $\epsilon(\rho) \to 0$ the Weierstrass integral maps the $+45^0$ segment to a curve that is on the *other* side of the plane $x_2 = 0$ as the horizontal half-line.

With our choices, the horizontal half-line is always the positive x_2-axis (see 5.3.2, 2.1.1), but it is a *fixed* half of the x_2-axis, i.e. independent of ρ, also under other sign conventions. Therefore our remaining proof will show

$$\begin{aligned} x_2(\wp_g = e^{i\rho}) > 0 &\quad \text{for } \rho \text{ near } \pi/2\ , \\ x_2(\wp_g = e^{i\rho}) < 0 &\quad \text{for very small } \epsilon(\rho) > 0. \end{aligned}$$

5.6 Details if ρ is near $\pi/2$.

5.6.1. Summary.

In this section it is convenient to scale the minimal surface by multiplying the dh in (5.3.2) by the real factor $(2/\cos\rho)^{1/2}$. Then we prove in (5.6.2):

(i) The length of each of the two horizontal segments from $(\wp_g = 0)$ to $(\wp_g = i)$ is ≥ 0.19 (if $\pi/4 \leq \rho < \pi/2$).

We also prove in (5.6.4), after estimating the Gauss map in (5.6.3):

(ii) The segments from $(\wp_g = i)$ to the branch points $(\wp_g = e^{i\rho})$ or $(\wp_g = -e^{-i\rho})$ have length $\leq \text{const} \cdot (\pi/2 - \rho)$.

For ρ close enough to $\pi/2$ this shows:

(iii) If we use the Weierstrass integral to map one half of the fundamental rhombus, say the one to the right of the vertical diagonal, then the branchpoints $(\wp_g = e^{i\rho})$ and $(\wp_g = -e^{-i\rho})$ are mapped to points in the x_1-x_2-plane which are on the *same* side of the x_1-axis as the initial segment of the horizontal diagonal.

5.6.2. The length estimate from below.

We use $\wp_g$ as coordinate function; i.e., the initial segment of the horizontal diagonal is given by

$$\wp_g = i \cdot t, \quad 0 \leq t \leq 1, \quad \frac{d\,\wp_g}{\wp_g} = dt.$$

With this we express dh from (5.3.2) (recall that we rescaled by $(2/\cos\rho)^{1/2}$) as follows:

$$|dh| = |t - \epsilon| \cdot (t + \frac{1}{t} - 2\sin\rho)^{-1/2}.$$

We do not use detailed information about the Gauss map, only that

$$|g| + \frac{1}{|g|} \geq 2.$$

Then:

$$\begin{aligned}
&\text{Length(segment from } (\wp_g = 0) \text{ to } (\wp_g = i))\\
&\geq 2 \int |dh|\\
&= 2 \int_0^1 |t-\epsilon|(t + \frac{1}{t} - 2\sin\rho)^{-1/2} dt\\
&\geq 2 \int_0^{\epsilon} (\epsilon - t)t(t^3 + t - 2t^2 \sin\rho)^{-1/2}\ dt\\
&\geq 2(\epsilon + \epsilon^2(\epsilon - 2\sin\rho))^{-1/2} \int_0^{\epsilon} (\epsilon - t)t\ dt\\
&\geq \frac{1}{3}\epsilon(\rho)^{2.5}\\
&\geq 0.19 \quad \text{(use } \pi/4 \leq \rho \text{ and (5.3.4)).}
\end{aligned}$$

5.6.3. The Gauss map estimate.
Again we use $\wp_g$ as coordinate map. The segment from the quarter-point on the horizontal diagonal ($\wp_g = i$) to the half-period point ($\wp_g = e^{i\rho}$) is then given by:

$$\wp_g = e^{i\varphi}, \quad \rho \leq \varphi \leq \pi/2, \quad \frac{d\,\wp_g}{\wp_g} = i \cdot d\varphi.$$

Along this segment we prove the
LEMMA

$$\max(|g|, \frac{1}{|g|})(\varphi) \leq \exp(46(1-\sin\rho)^{3/8} + 1)\sqrt{\frac{1+\epsilon^2 - 2\epsilon\sin\rho}{1+\epsilon^2 - 2\epsilon\sin\varphi}}.$$

PROOF. We have:

$$\log|g|(t) = \int_\rho^t \mathrm{Re}\,\frac{dg}{g}, \quad \rho \leq t \leq \pi/2.$$

We observe $e^{i\pi/4}du(e^{-i\pi/4}) \in \mathbb{R}$, therefore we can take the real part in the second formula for dg/g in (5.3.6). We leave the sign undetermined so that all four segments from $\wp_g = i$ perpendicular to the horizontal diagonal are included. We obtain

$$\mathrm{Re}(\frac{dg}{g}) =$$
$$\pm\,\epsilon\sqrt{\epsilon + \frac{1}{\epsilon} - 2\sin\rho}\Big(\mathrm{Re}\,\frac{1}{e^{i\varphi} - i\epsilon} + \mathrm{Re}\,\frac{e^{i\varphi} - i(X+\epsilon)}{Y}\Big)\frac{d\varphi}{\sqrt{2\sin\varphi - 2\sin\rho}}.$$

It is convenient that the real part gets rid of $(X+\epsilon)$ since Y is real. We will estimate the integrals involving the terms

$$\mathrm{Re}(\frac{1}{e^{i\varphi} - i\epsilon}) = \frac{\cos\varphi}{\cos^2\varphi + (\epsilon - \sin\varphi)^2} \quad \text{and } \frac{\cos\varphi}{Y}$$

separately and thereby get a bound for $\max(|g|, 1/|g|)$.
The term involving Y can be integrated:

$$\int_\rho^t \frac{\cos\varphi d\varphi}{\sqrt{2\sin\varphi - 2\sin\rho}} = \sqrt{2\sin t - 2\sin\rho}.$$

From $\sin\rho < \epsilon < 1$ (5.3.4) it follows that

$$2\epsilon(1-\sin\rho) < \epsilon^2 + 1 - 2\epsilon\sin\rho < 2(1-\sin\rho).$$

In (5.4) we proved

$$\frac{1}{23}(1-\sin\rho)^{5/8} \le Y.$$

This bounds the integral of the summand (of $\operatorname{Re} dg/g$) involving Y as follows:

$$\begin{aligned}
&\frac{\sqrt{\epsilon(\epsilon^2+1-2\epsilon\sin\rho)}}{Y}\int_\rho^t \frac{\cos\varphi d\varphi}{\sqrt{2\sin\varphi - 2\sin\rho}} \\
&\le 46(1-\sin\rho)^{3/8}\sqrt{\frac{\sin t - \sin\rho}{1-\sin\rho}} \\
&\le 46(1-\sin\rho)^{3/8}.
\end{aligned}$$

We now turn our attention to the other integral. Because it has a bad denominator coming from $\operatorname{Re} 1/(\wp_g - i\epsilon)$ if ρ is near $\pi/2$ we split this integral as follows:

$$\begin{aligned}
&\int_\rho^t \frac{\cos\varphi d\varphi}{(1+\epsilon^2-2\epsilon\sin\varphi)\sqrt{2\sin\varphi - 2\sin\rho}} \\
&= \int_\rho^t \frac{\cos\varphi d\varphi}{(1+\epsilon^2-2\epsilon\sin\rho)\sqrt{2\sin\varphi - 2\sin\rho}} \\
&\qquad + \int_\rho^t \frac{2\epsilon(\sin\varphi - \sin\rho)\cos\varphi d\varphi}{(1+\epsilon^2-2\epsilon\sin\rho)(1+\epsilon^2-2\epsilon\sin\varphi)\sqrt{2\sin\varphi - 2\sin\rho}} \\
&=: \int_\rho^t f_1(\varphi)d\varphi + \int_\rho^t f_2(\varphi)d\varphi.
\end{aligned}$$

The first term can be integrated as before and gives the contribution:

$$\begin{aligned}
&\sqrt{\epsilon(\epsilon^2+1-2\epsilon\sin\rho)}\int_\rho^t f_1(\varphi)d\varphi \\
&= \sqrt{\frac{2\epsilon(\sin t - \sin\rho)}{1+\epsilon^2-2\epsilon\sin\rho}} \\
&\le 1
\end{aligned}$$

In the second term we bound in the numerator

$$\sqrt{\sin\varphi - \sin\rho} \le \sqrt{\sin t - \sin\rho}$$

to get an explicitly integrable integrand:

$$\int_\rho^t \frac{2\epsilon\cos\varphi\ d\varphi}{1+\epsilon^2-2\epsilon\sin\rho} = \log\frac{1+\epsilon^2-2\epsilon\sin\rho}{1+\epsilon^2-2\epsilon\sin t}.$$

With this the contribution of the second term to the bound of the integral of $\operatorname{Re} dg/g$ is:

$$\begin{aligned}
&\sqrt{\epsilon(\epsilon^2+1-2\epsilon\sin\rho)}\int_\rho^t f_2(\varphi)d\varphi \\
&\le \frac{1}{2}\sqrt{\frac{2\epsilon(\sin t-\sin\rho)}{1+\epsilon^2-2\epsilon\sin\rho}}\cdot\log\frac{1+\epsilon^2-2\epsilon\sin\rho}{1+\epsilon^2-2\epsilon\sin t} \\
&\le \frac{1}{2}\log\frac{1+\epsilon^2-2\epsilon\sin\rho}{1+\epsilon^2-2\epsilon\sin t}.
\end{aligned}$$

Taking our three contributions together we get the bound of the lemma:

$$\max(|g|,\frac{1}{|g|})(t)\le\exp(46(1-\sin\rho)^{3/8}+1)\sqrt{\frac{1+\epsilon^2-2\epsilon\sin\rho}{1+\epsilon^2-2\epsilon\sin t}}.$$

QED

Note that the proof really gives the better bound 1 at $t=\rho$, but the more complicated expression distracts from what we need.

5.6.4. The remaining length estimate.

Along the segment from ($\wp_g = e^{i\rho}$) to ($\wp_g = i$) we introduced $\wp_g$ as coordinate, i.e. we have

$$\wp_g = e^{i\varphi},\quad \rho\le\varphi\le\pi/2,\quad \frac{d\,\wp_g}{\wp_g} = i\cdot d\varphi.$$

With this we express $|dh|$ from (5.3.2) (scaled as in (5.6.2) by $(2/\cos\rho)^{1/2}$) as follows

$$\begin{aligned}
|dh| &= \sqrt{\frac{1+\epsilon^2-2\epsilon\sin\varphi}{2(\sin\varphi-\sin\rho)}}d\varphi \\
&\le \sqrt{\frac{1+\epsilon^2-2\epsilon\sin\varphi}{2(1-\sin\rho)}}\sqrt{\frac{\pi/2-\rho}{\varphi-\rho}}d\varphi.
\end{aligned}$$

This bound for $|dh|$ and the preceding Gauss map estimate (5.6.3) imply the length estimate for our segment which was claimed in (5.6.1):

$$\begin{aligned}
&\int_\rho^{\pi/2}(|g|+\frac{1}{|g|})|dh| \\
&\le 2\exp(1+46(1-\sin\rho)^{3/8})\int_\rho^{\pi/2}\sqrt{\frac{\pi/2-\rho}{\varphi-\rho}}d\varphi \\
&\le 4\exp(1+46(1-\sin\rho)^{3/8})(\pi/2-\rho).
\end{aligned}$$

5.7 The behavior as $\epsilon(\rho) \to 0$.

To complete the intermediate value argument we will now show that, for small $\epsilon > 0$, the images of the branch points $\wp_g = e^{i\rho},\ -e^{-i\rho}$ lie in the (x_1, x_2)-plane on the opposite side of the x_1-axis as they do for ρ near $\pi/2$, discussed in (5.6). It is important to recall that we restrict the Weierstrass integral (2.1.1) to a simply connected portion of the punctured torus, to that half of the fundamental rhombus which is to the *right* of the vertical diagonal, because the 180^0 symmetry around the vertical line interchanges the sides of the x_1-axis. We also recall from (5.3.4) and (5.3.8):

There exists $\rho_+,\ -\pi/2 < \rho_+ < -\pi/6$ such that
$\epsilon(\rho_+) = 0$, and $\epsilon(\rho) > 0$ for $\rho \in (\rho_+, \pi/2)$;
if $\rho \to \rho_+$ then

$$X \to 0, \quad Y \to 1, \quad r \to -1, \quad E \to 1.$$

Our Weierstrass data become degenerate if $\epsilon = 0$ because the Gauss map cannot be unitary and vertical at the same point $\wp_g = 0 = i\epsilon$. But we can discuss the surfaces for ϵ close to 0. Using the definition of dg/g in (5.3.6) we conclude that

$$\lim_{\rho\to\rho_+} \frac{1}{\sqrt{\epsilon}}\frac{dg}{g} = -(\wp_g + \frac{1}{\wp_g})\sqrt{\frac{2}{\cos\rho_+}}(e^{+i\pi/4}du).$$

This shows that dg/g converges uniformly to 0 outside a neighbourhood of the horizontal diagonal (with its poles of dg/g); in particular this uniform convergence holds along those $+45^0$ segments which join the branch points of $\wp_g$ where $g = -1$ with the points $\wp_g = -i$ on the vertical diagonal. Without further estimates we thus have that along these segments the Gauss map converges uniformly,

$$g \to -1 \text{ as } \rho \to \rho_+.$$

From (5.3.2) we have

$$dh = (\wp_g - i\epsilon)(e^{-i\pi/4}du).$$

Again we choose $\wp_g$ as coordinate map; along the $+45^0$ segments from $\wp_g = -i$ we have

$$\wp_g = e^{i\varphi}, \quad |-\pi/2 - \varphi| \le |-\pi/2 - \rho|, \quad e^{-i\pi/4}du(e^{+i\pi/4}) = 1.$$

Now this controls the second coordinate differential of the Weierstrass integral:

$$\begin{aligned} dx_2 &= \operatorname{Re} i(g + \frac{1}{g})dh \to 2(\sin\varphi - \epsilon)(e^{-i\pi/4}du), \\ \text{error } &\le |g + \frac{1}{g} - 2||dh|, \end{aligned}$$

where we used the fact that $(e^{-i\pi/4}du)$ is real on the tangent vectors of the segments. We may assume $\rho < -\pi/6$; then $\sin\varphi < -0.5$ and the limit for

dx_2 shows that the second coordinate function of the minimal surface is strictly monotone along the segments considered (for ρ close enough to ρ_+). Finally, why does x_2 have *opposite* signs a) along these segments and b) on the horizontal half-line from $\wp_g = 0$, assuming that we integrate to the right of the vertical diagonal? The reason is that the x_2-coordinate remains zero along the vertical diagonal from $\wp_g = 0$ to $\wp_g = -i$, but the tangent plane rotates by approximately an *odd* multiple of π because $g = +1$ at $\wp_g = 0$ and $g \to -1$ at $\wp_g = -i$. This means that the initial tangent vector to the image of the $+45^0$ segment that starts at $\wp_g = -i$ points approximately in the *opposite* direction as the initial tangent of the horizontal half-line. The horizontal half-line and the Weierstrass image of the segment have to stay on *opposite* sides of the coordinate plane $x_2 = 0$ because of the monotonicity property that we have already established.
We proved: The x_2-coordinate of the Weierstrass image of the branch point, where $\wp_g = e^{i\rho}$, which is a continuous function of the conformal parameter $\rho \in (\rho_+, \pi/2)$ of the rhombic tori, has opposite signs if ρ is near the endpoints of $(\rho_+, \pi/2)$. Therefore, some ρ exists for which this function is zero; this says that the images of the branch points of $\wp_g$ are on the x_1-axis, i.e. on the *common* symmetry normal of these three points. Therefore the period condition is satisfied; we have found the Weierstrass data for which the Weierstrass integral is a well-defined map of the punctured torus into $\mathbb{R}^3$. The genus one helicoid exists.